UNIVERSITÉ DE SHERBROOKE

Faculté de génie
Département de génie électrique et de génie informatique

CHARACTERIZATION OF AMORPHOUS SILICON CARBIDE AND ITS APPLICATION TO CONTACT BARRIER DIODE

CARACTERISATION DE CARBURE DE SILICIUM AMORPHE ET SON APPLICATION À LA DIODE À BARRIERE DE CONTACT

Thèse de doctorat (Ph.D)
Spécialité : génie électrique

Professeur Çetin Aktik
Professeur Mihai Scarlete
Professeur Réjean Fontaine
Dr. Abdossamad Talebpour

TAHEREH FANAEI SHEIKHOLESLAMI

Sherbrooke (Québec), Canada Automne 2008

Your file Votre référence
ISBN: 978-0-494-48550-7
Our file Notre référence
ISBN: 978-0-494-48550-7

RÉSUMÉ

Des couches minces du carbure silicium amorphe ont été préparées en utilisant un procédé de déposition en phase vapeur ayant comme source des polymères (PS-CVD). Les couches ont été déposées à des températures qui varient entre 750 et 1000 °C. Les substrats utilisés pour les dépôts sont en silicium cristallin du type p et n, et en dioxyde de silicium (SiO_2) obtenu par croissance thermique. Les propriétés chimiques et électriques des couches ont été étudiées par diverses techniques, y compris la spectroscopie infrarouge par transformée de Fourier, détection de recul élastique (ERD), et la mesure de capacité-tension. Nous avons observé une corrélation entre la concentration moyenne de l'oxygène dans les films et la température de déposition, liant une faible concentration en oxygène dans le film à une température élevée de déposition. Cependant, la concentration de l'oxygène dans les films déposés à la même température était indépendante du substrat. Les couches minces déposées à basse température ont démontré un comportement isolant, alors qu'un comportement semi-conducteur est obtenu à température élevée. Des contacts ohmiques ont été obtenus sur la couche mince de carbure de silicium amorphe (a-SiC) en évaporant des contacts de nickel, suivis d'un recuit à 800 °C pendant 2 minutes. La mobilité de Hall moyenne obtenue est d'environ 34 $cm^2/V.s$ pour les échantillons déposés sur SiO_2 à 1000 °C.

Les caractéristiques générales du a-SiC déposé à 750 °C, ont été étudiées se servant des hétérostructures de SiC/c-Si utilisées comme des diodes à barrière de contact. Les propriétés de transport du courant dans la couche mince de a-SiC déposée sur un substrat de c-Si de type-p ont été étudiées en utilisant des mesures courant-tension (IV) et capacité-tension (CV). Les caractéristiques IV ont montré qu'une dépendance exponentielle du courant aux tensions est applicable pour les basses tensions tandis que la caractéristique de courant limité par les charges de l'espace est dominante pour les hautes tensions. Les caractéristiques de CV ont indiqué un comportement de type-p pour a-SiC résultant de la charge positive injectée par le substrat de silicium. La mobilité des trous et la durée de vie des porteurs injectés dans la couche mince de a-SiC ont été calculées en utilisant un modèle du courant limité par les charges d'espace. La variation de la mobilité effective des trous de a-SiC varie entre 10^{-4} et

10^{-7} et attribuée aux diverses valeurs de la densité des défauts dans les couches minces de a-SiC.

ABSTRACT

Thin films of amorphous silicon carbide were prepared using Polymer-Source Chemical Vapor Deposition (PS-CVD) at temperatures between 750 and 1000 °C. The substrates were silicon single crystal wafers of p-type and n-type, and thermally-grown silicon dioxide substrates. The chemical and electrical properties of the films were studied by various techniques, including Fourier-transform infrared spectroscopy, Elastic Recoil Detection (ERD), and capacitance-voltage technique. A correlation was observed between the average concentration of oxygen in the films and the deposition temperature, linking a low oxygen concentration in the film to a high deposition temperature. However, the concentration of oxygen in the films deposited at the same temperature was independent of the substrate. The thin films deposited at low temperature showed insulating behaviour, while the semiconducting behaviour was obtained at high deposition temperatures. Ohmic contacts were obtained on the deposited a-SiC thin film by evaporating nickel contacts, followed by annealing of the sample at 800 °C for 2 minutes. The average Hall mobility was found about $\mu_H = 34\ cm^2/V.s$ for the samples deposited on SiO_2 substrate at 1000 °C.

The general characteristics of wide band gap a-SiC deposited at 750 °C, was studied using a-SiC/c-Si heterostructures applied as the contact barrier diodes. The current transport properties of a-SiC thin film deposited on a p-type silicon c-Si substrate were investigated using current-voltage (IV) and capacitance-voltage (CV) measurements. IV characteristics showed an exponential dependence of current to the applied voltages for low forward bias while the space charge limited current characteristics dominated for higher forward bias. CV characteristics indicated a p-type property for a-SiC which is resulted by the injected positive charge from p-type silicon substrate. The hole mobility and injected carrier lifetime in a-SiC thin film was calculated using a model of space-charge limited current. The variation in effective hole mobility of a-SiC, which was ranged between 10^{-4} and 10^{-7}, was attributed to the various values of defect density of the a-SiC thin films.

REMERCIEMENTS

Je tiens à exprimer ma plus profonde reconnaissance à mon directeur et co-directeur de thèse, le professeur Çetin Aktik et le professeur Mihai Scarlete, pour leurs conseils précieux et éclairés.

Je voudrais remercier les membres du Jury d'avoir accepté d'examiner ce travail.
Je voudrai aussi remercier tous ceux et celles qui ont contribué, de près ou de loin à l'aboutissement de ce travail. Je voudrais remercier les membres de la compagnie Sixtron en particulier Mme. Nathalie Camiré pour la préparation des échantillons. Je voudrais remercier tous les techniciens de salle blanche pour leur aide pendant la caractérisation des échantillons. Je voudrais remercier Dr. Subhash Gujrathi pour sa contribution dans la caractérisation chimique. Je voudrais remercier tous mes collèges en particulier M. El Hassane Oulachgar pour les discussions techniques.

Enfin, je voudrai exprimer ma reconnaissance à mon mari, professeur Amin Behzadmehr pour son grand support technique et moral tout au long de mes études, et ma grande famille en Iran pour le grand appui moral qu'elle a su m'apporter.

CONTENTS

CHAPTER 1: INTRODUCTION 1

CHAPTER 2: BIBLIOGRAPHY 5

2.2. EFFECT OF DEPOSITION CONDITIONS 8
2.3. TRANSPORT PROPERTIES OF A-SIC 10
2.4. A-SIC/C-SI HETEROJUNCTION 11
2.5. APPLICATIONS OF A-SIC 14
2.5.1. OPTOELECTRONIC DEVICES 14
2.5.2. PASSIVATION LAYERS 16
2.5.3. COATING MATERIAL 17

CHAPTER 3: AMORPHOUS MATERIALS 19

3.1. MOBILITY OF CHARGE CARRIERS IN AMORPHOUS MATERIALS 20
3.2. APPLICATION OF AMORPHOUS MATERIALS IN CONTACT BARRIER DIODE 22
3.2.1. ROLE OF THE AMORPHOUS INTERLAYER 23
3.2.2. CAPACITANCE-VOLTAGE CHARACTERISTICS 23
3.2.3. CURRENT-VOLTAGE CHARACTERISTICS 25

CHAPTER 4: EXPERIMENTAL DETAILS 31

4.1. PREPARATION OF A-SIC 31
4.2. CHARACTERIZATION METHODS 32
4.2.1. ERD MEASUREMENTS 33
4.2.2. HALL MEASUREMENTS 33

CHAPTER 5: MATERIAL CHARACTERIZATION AND DISCUSSION 37

5.1. MATERIAL CHARACTERIZATION 37
5.2. CONTACT CHARACTERIZATION 47
5.3. RESULTS OF MOBILITY MEASUREMENTS 49

CHAPTER 6: APPLICATION OF A-SIC LAYERS IN CONTACT BARRIER DIODES 51

6.1. IV CHARACTERISTICS 54
6.2. CV CHARACTERISTICS 58
6.3. MOBILITY AND LIFETIME CALCULATION 62

REFERENCES.....72

LIST OF FIGURES

Figure 2-1 An example of IR spectrum of a-SiC films

Figure 2-2 Various possible configurations of CH_3 groups attached to silicon in a-$Si_{1-x}C_x$:H films. Note that Y is either Si or C, not attached to three hydrogen atomes

Figure 2-3 The absorption strength of the main IR absorption bands as a function of carbon-content (x). Note that the two Si-H curves and the Si-C and Si-CH_3 curves are based on the deconvolution of the corresponding absorption peaks into Gaussian subpeaks

Figure 3-1 Models illustrating the structure of (a) crystalline and (b) amorphous materials

Figure 3-2 Room temperature capacitance voltage characteristics of undoped a-Si:H/p-c-Si ($N_A = 10^{16}\ cm^{-3}$) heterojunction

Figure 3-3 Current-voltage characteristics of undoped a-Si:H/p-c-Si ($N_A = 10^{16}\ cm^{-3}$) heterojunction

Figure 4-1 The arbitrary shaped samples for Hall measurements: (a) and (b) acceptable to determine the carrier concentration, carrier type, resistivity, and mobility, (c) recommended only for mobility measurement

Figure 5-1 FT-IR spectra in the 500-1500 cm^{-1} region of thin film deposited at temperatures of 750, 850, 950 and 1000 °C on (a) n-type silicon substrate, (b) p-type silicon substrate, and (c) silicon dioxide thermally grown on silicon substrate

Figure 5-2 ERD measurement of thin film deposited at 750 °C on (a) n-type silicon substrate, (b) p-type silicon substrate, and (c) silicon dioxide thermally grown on silicon substrate

Figure 5-3 Oxygen concentration in the films deposited at temperatures of 750, 850, 950 and 1000 °C on SiO_2 substrate

Figure 5-4 Oxygen concentration in the films deposited at temperatures of 750, 850, 950 and 1000 °C on SiO_2 substrate

Figure 5-5 CV curve of thin film deposited at 750 °C, 850 °C, and 950 °C on n-type silicon substrate

Figure 5-6 CV curve of thin film deposited at 750 °C, 850 °C, and 950 °C on p-type silicon substrate

Figure 5-7 CV curve of thin film deposited at 750 °C, 850 °C, and 950 °C on silicon dioxide substrate

Figure 5-8 CV curve of thin film deposited at 1000 °C, (a) on n-type silicon, (b) on p-type silicon, (c) on silicon dioxide

Figure 5-9 Current-voltage characteristic of nickel contact of deposited thin film at 1000 °C (a) before annealing, (b) after annealing

Figure 5-10 ERD measurement of thin film deposited at 1000 °C on SiO_2 substrate

Figure 6-1 ERD depth profiles of elements in Ni/a-SiC/p-Si/Al diodes for the thickness of a-SiC layer; a) 215 nm, b) 270 nm, and c) 270 nm

Figure 6-2 IV characteristic for the three Ni/a-SiC/p-Si samples. Two samples have 270 nm a-SiC, and one other has 215 nm a-SiC

Figure 6-3 Low voltage region of the IV curves used for saturation currents and ideality factors calculation

Figure 6-4 Forward current characteristic on a log-log scale of the Ni/a-SiC/p-Si devices

Figure 6-5 CV characteristic for the three Ni/a-SiC/p-Si samples. Two samples have 270 nm a-SiC, and one other has 215 nm a-SiC

Figure 6-6 A^2/C^2 vs. voltage for the Ni/a-SiC/p-Si heterostructures

Figure 6-7 Equivalent circuit of contact barrier diode

Figure 6-8 Effective mobility of a-SiC (μ_{eff}) vs. applied voltage (V_a) for higher forward biased Ni/a-SiC/p-Si contact barrier diodes

Figure 6-9 Effective mobility of a-SiC (μ_{eff}) vs. applied voltage (V_a) for higher lower biased Ni/a-SiC/p-Si contact barrier diodes

Figure 6-10 Voltage drop across the organic layer (V_{sc}) vs. applied voltage (V_a) for Ni/a-SiC/p-Si devices

Figure 6-11 Lifetime of injected carriers (τ) vs. applied voltage (V_a) for higher forward biased Ni/a-SiC/p-Si contact barrier diodes

Figure 6-12 Lifetime of injected carriers (τ) vs. applied voltage (V_a) for lower forward biased Ni/a-SiC/p-Si contact barrier diodes

Figure 6-13 Electric field in the space-charge layer (E_{sc}) and in the substrate (E_{si}) of Ni/a-SiC/p-Si contact barrier diode

LIST OF TABLES

TABLE 4-1 DEPOSITION CONDITIONS FOR A-SIC THIN FILMS

TABLE 6-1 ELECTRICAL PROPERTIES OF NI/A-SIC/P-SI CONTACT BARRIER DIODES OBTAINED FROM IV ANALYSIS

TABLE 6-2 ELECTRICAL PROPERTIES OF NI/A-SIC/P-SI CONTACT BARRIER DIODES OBTAINED FROM CV ANALYSIS

CHAPTER 1: INTRODUCTION

The thin films are the key elements for continued technological advances in the fields of electronic, photonic, and magnetic devices. The synthesis of materials as thin films enables easy integration of various types of devices. The thin film modules are expected to be cheaper to manufacture owing to their reduced material, energy, handling and capital costs. The introduction of large area thin film amorphous semiconductors with low cost fabrication capability has not only given a new impetus to the field of optoelectronic devices, such as solar cells, flat panel displays, image sensors or printer heads, but it now also forms the basis for large area of microelectronic devices. The amorphous semiconductors lack long rang ordering of their constituent atoms, but they do have local order on the atomic scale. This short range order is directly responsible for observable semiconductor properties such as optical absorption edges and activated electrical conductivities. The discovery of the ability to control the optical band gap energies by alloying silicon with other elements has introduced a new phase in the field of amorphous semiconductors.

One of the promising materials for various applications in opto- and micro-electronic devices is the thin film amorphous silicon carbide (a-SiC). This thermally and chemically stable wide band gap material has superior mechanical strength, high radiation resistance and high optical transmittance [NELSON et al., 1966, DEMISHELIS et al., 1991, El KHAKANI et al., 1993]. The preparation methods and the deposition conditions have a significant effect on electrical properties of a-SiC such as conductivity and transport prosperities. For example, thin films of a-SiC with the band gap larger than 1.9 eV require the inclusion of larger amounts of carbon. The increasing of carbon content in the film leads to a higher increased midgap state density and limits the transport properties of the undoped a-SiC. Moreover, it is difficult to add impurity as doping to the wide band gap a-SiC due to the high localized tail density of states associated with both band edges and midgap state density [KANICKI, 1991].

Recently, SiC has been prepared using different deposition or growing methods. Chemical vapour deposition (CVD) is a widely used technique for the preparation of crystalline and

polycrystalline silicon carbide. Very high temperatures (1400-2200 °C) are needed for the preparation of crystalline SiC from gas mixtures that contain molecules such as $SiCl_4$, CH_4, H_2, or $H_3C+SiCl_3$ [SCHLICHTING, 1980]. Microcrystalline SiC can be obtained at temperatures below 1200 °C [O'CONNOR et al., 1960]. The possibility of preparing a-SiC films by CVD method using simple molecules such as $SiCl_4$ and CH_4 was studied by Bullot et Schmit [BULLOT et al., 1987]. but only the simple molecule such as CH_4, $SiHCl_3$, $SiCl_4$, and HCl were detected in presence of hydrogen. Thus, it was concluded that this method is not suitable for preparing a-SiC films. The decomposition reactions of several more complicated organosilicon compounds for the deposition of a-SiC films has been reported [GERAULT et al., 1982, GERAULT et al., 1983, GERAULT et al., 1984]. The films prepared by the decomposition of these organosilicon compounds contained between 24 and 82 percent silicon, depending on the source gas and the substrate temperature. Plasma-enhanced chemical vapor deposition (PECVD) has become the most commonly used method in the a-SiC film deposition. It was found that the structure of the a-SiC thin films grown on Si-substrates depends strongly upon the deposition condition such as source, substrate temperature, pressure, etc. [CHO et al., 2002]. The majority of deposition systems currently used are capacitively coupled and the gas mixture is SiH_4 + CH_4. The substrate temperature is mostly in the range of 200 to 300 °C, and the pressure is 0.1 to 1 Torr. There are wide variations in the power used in these systems [CHOI, 2001, CHO et al., 2006, TAKAHASHI et al., 1997, EICKHOFF et al., 2004]. This method is associated with high preparation costs, involves relatively expensive equipment, and is a time-consuming procedure [SHIOZAWA et al., 1995]. Because of the interesting properties of the a-SiC thin film, the economic interest in the production of this material is high and needs to look for a lower cost method. Alternatively, polymeric precursors have been used to synthesize silicon carbide [KHO et a., 2001, RAMAKRISHNAN et al., 2001, DISMUKES et al., 1997]. Further, in a relatively recent development [SCARLETE et al., 2003], polysilane precursors have been used in the Polymer-Source Chemical Vapor Deposition (PS-CVD) method to synthesize thin films of a-SiC. The most significant advantage of the PS-CVD method is the high deposition rate resulting from a) the *in situ* synthesis in the reactor of the gaseous ceramic precursors with the highest known density to date (around 300 a.m.u.), and b) the involvement of a specific fast mechanism of synchronized SiC bonds rearrangement [SCARLETE et al., 1994,

SCARLETE et al., 1995]. Additional advantages of the PS-CVD method are the simplicity of the equipments and handling procedures due to the deposition at atmospheric pressure, which eliminates the requirements for expensive equipment imposed by classic CVD methods. In addition, the operation involves a reasonably stable precursor and reduced health hazard [SCARLETE et al., 2003].

DC conductivity of a-SiC films consists of hopping conduction in the conduction band tail plus tunnelling from localized states to the dangling bond defects [BULLOT et al., 1987]. The activation energy for the extended state conduction (ΔE_1) is defined as $\Delta E_1 = E_c - E_F$, where E_c is the conduction band edge and E_F is the Fermi energy level. The activation energy for the hopping conduction (ΔE_2) can then be expressed as $\Delta E_2 = E_A - E_F + W$ [MOT et al., 1979], where E_A is the conduction band tail edge and W is the hopping activation energy of electrons in the band tail. Therefore, the band tail width increases upon carbon incorporation, which means that carbon incorporation increases disorder in these alloys [RIZK et al., 1987]. The undoped samples of a-SiC exhibit a single activation energy that is consistent with conduction via the extended states [DEMICHELIS et al., 1991]. The conductivity of doped samples at high temperatures corresponds to the extended states but near the room temperature the transport mechanism occurs by phonon-assisted hopping. The electrical properties of a-SiC could be investigated using a-SiC/c-Si heterostructures [MEGAFAS et al., 1992, MARSAL et al., 1997, MARSAL et al., 1999, CHOI et al., 2000]. This heterostructure shows the rectifying property over a large voltage range. The characterization results are used to explore some electrical properties of a-SiC such as dielectric constant, impurity concentration, electron affinity, breakdown voltage, mobility, and lifetime. The electron and hole mobility of a-SiC have been already measured using Hall measurements [NEBEL et al., 1993], time-of-flight technique [BAYLAY et al., 1993, GU et al., 1994] and photomixing technique [TANG et al., 1995]. The electron mobility of a-SiC was reported to be between 1 to 10 $cm^2V^{-1}s^{-1}$ and the hole mobility ranged from 1×10^{-4} to 3×10^{-3} $cm^2V^{-1}s^{-1}$.

The aim of this work is to characterize a-SiC as a wide band gap material, in order to investigate the performance of contact barrier microelectronic devices. The a-SiC thin films have been prepared by PSCVD method. The major electrical characterization techniques

used in this work were IV and CV measurements. The transport properties of undoped a-SiC were studied directly by the Hall measurement technique and indirectly by using a heterostructure device. The characterization results were used to analyze the properties of the contact of a-SiC/c-Si, such as the ideality factor and barrier height. An immediate objective was to investigate some properties of the amorphous layer itself, such as dielectric constant, injected carrier lifetime and mobility.

This thesis will be presented the electronic properties of intrinsic a-SiC, and the potential application of this material in contact barrier devices. Chapter 2 is a review of the recent researches on the electrical properties and device application of a-SiC material. The theoretical aspects of amorphous materials, properties and characterization methods are presented in the chapter 3. In chapter 4, the experimental methods used in this work for preparation and characterization of a-SiC thin film are explained. The results of material characterization and application in the contact barrier devices together with the calculation results are presented and discussed in chapters 5 and 6. Finally, a conclusion section summarizes the important points provided in this work.

CHAPTER 2: BIBLIOGRAPHY

The optical and electrical properties of amorphous silicon-carbon (a-SiC) alloys were reported for the first time in 1968 by three groups [MAGOB et al., 1968, HERMAN et al., 1968, WEINREICH et al., 1968]. Since then, intense research has been carried out on a-SiC films because of its potential applications in electronics and optical devices. The first review on the physics of a-SiC was published by Bullot and Schmit [BULLOT et al., 1987], based on data published between 1968 and 1987. Another review on a-SiC film developments was presented by Choi [CHOI, 2001], based on publications which have been reported between 1987 and 2000.

A survey of papers on a-SiC films published over the last 30 years shows that the majority of such films were prepared by the PECVD method, using a mixture of silane and methane (SiH_4+CH_4) gases, with or without hydrogen (H_2) dilution. The second most common deposition technique is sputtering. The unhydrogenated films are usually prepared by sputtering a polysilicon SiC target using argon (Ar). a-SiC films can be obtained by sputtering a crystalline silicon (c-Si) target in a CH_4+Ar atmosphere, or by sputtering a polycrystalline SiC target in an Ar+H_2 atmosphere. Two other preparation techniques for a-SiC are electron cyclotron resonance chemical vapour deposition (ECR-CVD) and photoinduced chemical vapor deposition.

Structural properties of a-SiC were studied by many researchers. The structural analysis methods which were frequently employed for the characterization of a-SiC films were the FT-IR, Raman, X-ray photoelectron, and Auger electron spectroscopy [WEIDER et al., 1987, CROS et al., 1992]. A detailed analysis of IR results obtained on a-SiC is presented in section 2.1. The effect of deposition conditions, as an important domain in a-SiC material, is a subject considered in section 2.2. A brief review on the transport properties of a-SiC is presented in section 2.3. The studies in transport properties of a-SiC using the junction of this material with crystalline semiconductors in terms of heterojunction are discussed in section 2.4. In the last section, some of the recent applications of a-SiC in optical and electrical devices will be presented.

2.1. IR spectroscopy of a-SiC

One of the commonly used techniques in the structural characterization of amorphous silicon carbide films is the Infrared spectroscopy [CHOI, 2001]. Figure 2-1 shows an IR spectrum of a-SiC films with characteristic peaks.

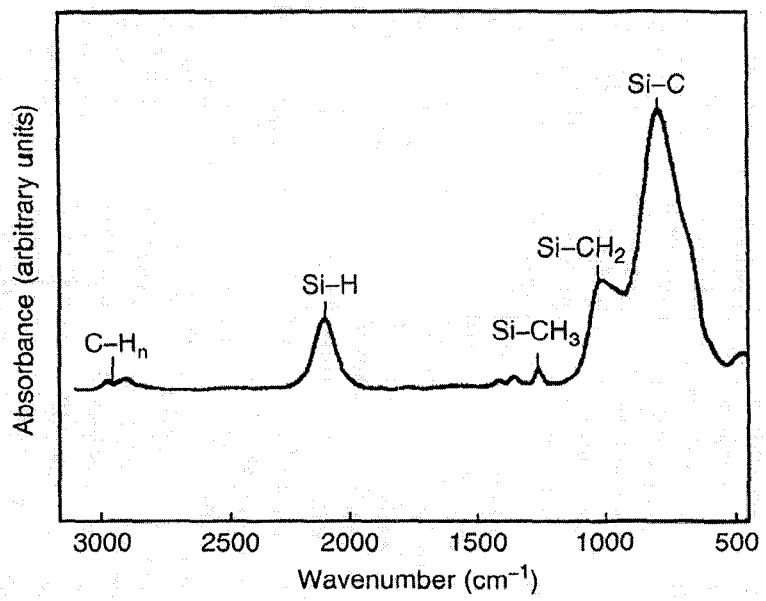

Figure 2-1 An example of IR spectrum of a-SiC films [MASTELARO et al., 1997]

The Si-C bond is partly ionic, and, therefore, IR absorption bands are expected for SiC vibrations. The broad peak between 700 and 800 cm^{-1} can be attributed to the Si-CH_3 rocking and to Si-C stretching mode. The peak at 900-1100 cm^{-1}corresponds to the C-H_n wagging mode. The peak at 1250 cm^{-1} corresponds to the Si-CH_3 bend. The peak at 2100 cm^{-1} is due to the Si-H_x stretching modes. The C-H_n stretching modes are at identified around 2900 cm^{-1}. Wieder et al. [WIEDER et al., 1979] estimated the composition dependence of the absorption strength of the Si-C bonds from a simple effective charge model. The possible configurations of how the CH_3 groups are attached to silicon are shown in figure 2-2 [WIEDER et al., 1979]. Bullot and Schmidt indicated that mixing rocking or wagging vibrations with the Si-C stretching mode enhances the absorption strength because the C_3 symmetry of methyl groups is slightly perturbed by a random distribution of second neighbour atoms. This is particularly

important for the Si-CH_3 rocking mode, because without this, it will not be mixed with the stretching mode. The CH_3 wagging mode has rocking mode only in configuration (c) of figure 2-2, but it could be mixed in configurations (a) and (b).

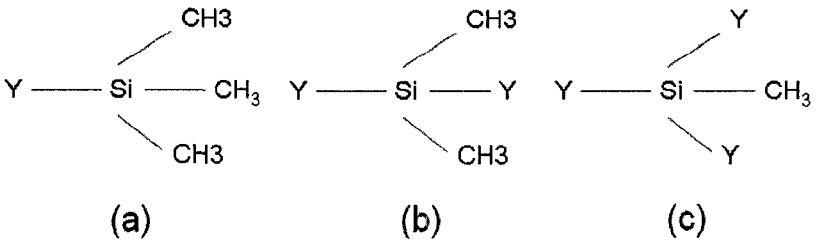

Figure 2-2 Various possible configurations of CH_3 groups attached to silicon in a-$Si_{1-x}C_x$:H films. Note that Y is either Si or C not attached to three hydrogen atomes [WIEDER et al., 1979]

Mode coupling is responsible for the shift of the wagging band and the Si-C stretching band with film composition. Figure 2-3 plots the composition dependence of the integrated absorption strength of the main IR absorption bands [WIEDER et al., 1979]. It could be seen from this figure that the Si-C and Si-CH_3 rocking and wagging modes at 670 and 780 cm^{-1} have different maxima as a function of x. The 780 cm^{-1} band appears only at carbon content over 10%. At the low carbon content the carbon atoms are incorporated into the silicon network and are mostly bonded to silicon. The absence of C-H absorption bands in the low carbon content range may be due to the weak absorption coefficient of the C-H bonds. According to Wieder et al. [WIEDER et al., 1979], at the low carbon content of a-$Si_{1-x}C_x$:H, the total hydrogen content increases between x=0 and x=0.3 because at this range, carbon atoms that are incorporated into the silicon network are always hydrogenated (CH or CH_2).

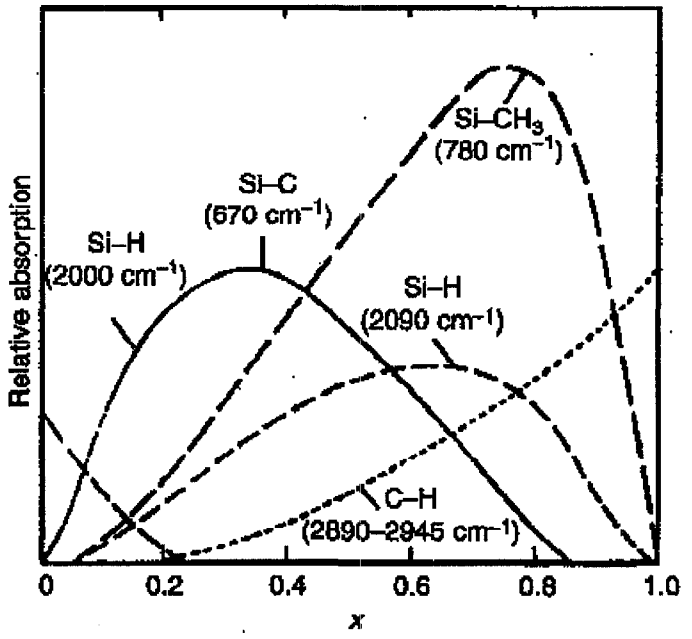

Figure 2-3 The absorption intensity of the main IR absorption bands as a function of carbon-content (x). Note that the two Si-H curves and the Si-C and Si-CH_3 curves are based on the deconvolution of the corresponding absorption peaks into Gaussian subpeaks [WIEDER et al., 1979]

2.2. Effect of deposition conditions

It is known that deposition conditions have significant effects on structural, electrical and optical properties of a-SiC. The recent studies on the deposition of a-SiC films using PECVD method include [MAHAN et al., 1985, MATSUDA et al., 1986, FOLSCH et al., 1992, LIN et al. 1987, SCHIFF et al., 1993]: The thin films of a-SiC with the band gap larger than 1.9 eV required the inclusion of larger amounts of carbon. However, as the band gap increases beyond 2 eV, the optoelectronic properties degrade and the Urbach energy and the sub band gap density of states or defects increase. This precluded the use of such materials in solar cells, tandem junction configuration or light emitting devices since the extra defects within the material act as efficient recombination centers. The addition of H_2 to $SiH_4 + CH_4$ plasma led to better optoelectronic properties, due to the increased energy gap, while the Urbach energy decreases results in increasing of the photoconductive gain. If the baseline material,

which has been deposited without hydrogen dilution, already shown good optoelectronic properties, the hydrogen dilution could be quite inefficient. Deichelis et al. [DEICHELIS et al., 1995] presented a method for establishing the optimum deposition conditions for a pure SiH_4 + CH_4 plasma in order to obtain a good quality baseline a-SiC:H material, by using an analytical method. They studied the effects of the CH_4 flow, substrate temperature and the pressure on the optoelectronic properties of deposited films. They found that the optimized conditions were achieved at 20 sccm CH_4 flow, 325 °C substrate temperature, and the pressure in the range 0.4-1 Torr. Under these conditions, they obtained optimized films of a-SiC:H with energy gap in the rage of 1.84-1.9 eV, Urbach energies below 60 meV, and photoconductive gain higher than 10^6 cm^2V^{-1}.

The effects of the deposition conditions on the transport properties of a-SiC has been studied by various research groups [KLAZES et al., 1982, LI et al., 1993, LI et al., 1992, LU et al., 1993]. Tang and Braunstein [TANG et al., 1995] determined the electron drift mobility, lifetime, and the conduction band Urbach energy of the rf glow discharge of prepared a-SiC films, as a function of hydrogen dilution ratio ($H_2/(CH_4+SiH_4)$). They indicated that by increasing the hydrogen dilution ratio from 0 to 25, the band gap energy decrease from 1.94 to 1.9 eV, the electron drift mobility and lifetime increase from 4 to 7 cm^2/Vs and 25 to 100 ns, respectively, and the Urbach Energy decrease from 47 to 43 meV. They concluded that for a-SiC:H films with increased hydrogen dilution ratio, the density of positively charged defects, negatively charged defects, and neutral defects all show a tendency to decrease.

Jung et al. [JUNG et al., 2003] deposited a-SiC on c-Si substrate by RF PECVD and by the thermal metal organic chemical vapor deposition (MOCVD) methods using a SiH_4 + CH_4 gas mixture and a single molecular precursor of diethylmethylsilane, respectively. They studied the effect of deposition parameters, such as deposition temperature, pressure, RF power, and annealing temperature on the structural and optical properties of a-SiC thin films. They realized that there were large variations in hydrogen contents and crystallinity in the films depending on the deposition and annealing temperatures. They indicated that the composition of films is changed from amorphous to polycrystalline and crystalline by increasing the deposition temperature from 700 to 1000 °C while the hydrogen content was decreased. It

was indicated that RF power is a main parameter for which the optical band gap is influenced rather than the annealing temperature. By increasing the RF power, the optical band gap energy increased from 3.68 to 4.09 eV, while the annealing temperature had no effect on the band gap energy. The FTIR result showed that the microcrystalline phase in the films was rapidly enhanced as the annealing temperature increased.

Like other properties, the dielectric constant of a-SiC can be affected by the deposition conditions. a-SiC is a potentially attractive low-k material due to its high electrical resistivity and its good thermal stability, both resulting from its highly cross-linked structure [ENDO et al., 1996, UOKOMICHI et al., 1998, CHO et al., 2000]. To reach lower k values, larger and more complex precursors, perhaps with cyclic molecular structure and more complex organic content, may be used to form cyclic structures with large open spaces inside the film. Li et al. [LI et al., 2003] used the PECVD technique with sources gases CH_4, SiH_4 and H_2 at room temperature and determined the deposition conditions that can lead to a-SiC films with lower dielectric constants. The dielectric constants were calculated from the high frequency (1 MHz) capacitance, measured on a metal-insulator-semiconductor structure formed with Au dot electrodes deposited on top of a-SiC by e-beam evaporation. The dielectric constants of the as-deposited films were found to vary with the RF power and CH_4 gas flow ratio. The lowest dielectric constant obtained was 2.71, for films deposited at RF power of 70 W and flow rate of 30:50:50 sccm for CH_4:SiH_4:H_2, respectively. They determined the mass density from X-ray reflectivity measurements to be about 1.353 g cm^{-3}. This value is smaller than the mass densities of SiO_2 and SiC. They mentioned that the prepared film had nearly 77% C atom obtained using X-ray photoelectron spectroscopy. UV Raman scattering indicated that C-C bond was principle in the film. The C rich SiC film with a density of ~1.353 gcm^{-3} was depicted as an inorganic C-C network in short range with internal surface of Si-OH or Si-C bonds.

2.3. Transport properties of a-SiC

The electronic transport of a-SiC has been investigated by different groups [ADRIAENSSENS et al., 1993, VON DER LINDEN et al., 1992, WANG et al., 1993].

Bayley et al. [BAYLEY et al., 1993] (1993) employed the time-of-flight (TOF) experiment over a wide range of temperatures and fields. The a-SiC thin films were deposited on glass substrate using RF glow discharge technique at the low power regime. The band gap energy was varied between 1.68 to 2.04 eV by increasing the carbon concentration. The electron drift mobility was estimated for these materials between 1 and 10 $cm^2V^{-1}s^{-1}$. It should be mentioned that the difficulty of applying TOF method to a-SiC is due to the trapping of photogenerated charges into a high density of mid gap states. In additions, increasing carbon content increases the density of deep level states. Nebel and Street [NEBEL et al., 1993] investigated the Hall measurements of n-doped a-SiC with varying carbon contents. The Hall mobility was found to decrease with increasing doping or carbon concentration. Then, the Hall mobility of a-SiC:H (0.02 to 0.06 $cm^2/V.s$) was shown to be lower than that of intrinsic a-Si:H ($\cong$ 0.15 cm^2/Vs). It was indicated that the Hall mobility is significantly smaller than the drift mobility and the Hall mobility of holes is about half that for electrons. Hole drift mobility of a-SiC was also measured by Gu et al. [GU et al., 1994] using photocarrier TOF technique. They prepared a-SiC using plasma deposition of hydrogen-diluted methane/silane mixtures. It was found that, as the band gap augments (from 1.72 to 1.91 eV), the hole drift mobility remains constant (about 2×10^{-3} cm^2/Vs).

2.4. a-SiC/c-Si heterojunction

Many results have been published on heterojunctions between amorphous SiC and single crystalline semiconductors, leading to application of this material in thin film transistors (TFT), metal-amorphous silicon FETs (MASFET) and heterojunction bipolar transistors (HBT). a-SiC material has been used to enhance the conversion efficiency of amorphous solar cells, as the emitter-base in high frequency Si heterojunction bipolar transistors and in thin film light-emitting diodes. a-SiC/c-Si heterojunction could be used to extract the transport properties of a-SiC material.

Magafas et al. [MEGAFAS et al., 1992] have investigated the electrical properties and the carrier transport mechanisms of a-SiC (Eg=1.36 eV)/c-Si heterojunction. a-SiC was deposited with RF sputtering on p-type c-Si substrate with Au at its back side and different

metals on the surface of a-SiC thin film as ohmic contacts. Result of CV plot shows the n-type conductivity for undoped a-SiC. The dielectric constant of a-SiC was estimated at about 11. Two different slopes in IV curves were observed, indicating two different transport mechanisms. The change in slope of log IV diagrams was observed above a temperature dependant critical value for the forward bias (V_T). They indicated that this phenomenon corresponds to a situation where the quasi-Fermi level of a-SiC and the conduction band edge of c-Si have the same energy. At low temperature and for forward-bias voltages greater than V_T, the tunnelling transport mechanism dominates and electrons from localized states near the Fermi level of a-SiC tunnel through the energy barrier into the conduction band of c-Si. In this study, Magafas et al. didn't consider the transport of holes from c-Si (p) into a-SiC, because they have found a much higher potential barrier for holes than the electrons and also because of the lower concentration of holes in p-Si than that of electrons in a-SiC, an assumption based on the results from capacitance measurements. An ideality factor of 1.5 was obtained for this heterojunction at temperatures lower than 250 K. It was suggested that the recombination transport mechanism is the dominant factor at temperatures lower than 250 K, whereas, at higher temperatures, the recombination-diffusion transport mechanism becomes dominant at high temperatures (higher than 250 K). From CV measurements, a value for the electron affinity $\chi = 4.12 \pm 0.04$ eV was calculated for a-SiC.

Marsal et al. [MARSAL et al., 1997] analysed the electrical properties of n-type a-SiC on p-type c-Si heterojunctions by measuring current-voltage characteristics. Two distinct regions were observed in measured forward current. In the low forward region, the behaviour was described by an exponential function and explained to be due to the recombination in the space charge region. At higher forward biases, they believed that an important part of the applied voltage falls in the quasi-neutral bulk region of the a-SiC layer. Therefore the characteristic deviates from the exponential behaviour and the current becomes space charge limited. The mobility gap of a-SiC was about 1.95 eV. The ideality factor and the saturation current obtained in the low voltage region (V<0.4 V) were n=1.3 and $I_o=6.3\times10^{-9}$ A, respectively. The value of the ideality factor was explained by a recombination mechanism in the amorphous phase, in terms of the existence of a high density tail states in this phase. Inspecting the log-log scale of the IV characteristics indicated that the current is not limited

by the resistance of the a-SiC layer and superlinearly increase at higher voltages (V>0.4 V). The superlinear or power-law dependence between current and voltage is characteristic of space-charge limited currents (SCLC). At the reverse bias, the higher current than what expected for a mechanism of generation in the depletion region, was explained by a tunnelling model. Marsal et al. used the space charge limited currents in this heterojunction to determine the density of states in the n-type a-SiC gap. The later results showed the increase in the localized states when approaching the conduction band edge.

Chew et al. [CHEW et al., 2001] used a structure of a-SiC/n-type c-Si heteojunction to investigate the density and distribution of gap states in a-SiC using high-frequency steady state capacitance-voltage measurement. The a-SiC films was grown by electron cyclotron resonance CVD technique. In their work, a-SiC was considered as the insulating layer. The reason for this was the measurement frequency of 1 MHz, which was set at three orders higher than the cut-off frequency. Such a film could be treated as dielectrics which do not respond to the ac signal and contribute only to the total capacitance by a constant value, independent of the voltage applied. For this treatment, a typical value of the conductivity for the undoped a-SiC films was 1×10^{-9} $(\Omega cm)^{-1}$ at the room temperature, and the dielectric constant of the film was assumed to be approximately 4-10. In further measurements, a value of 4.02 was confirmed for the a-SiC dielectric constant. The mid-gap density near the Fermi level was found to be 3×10^{15} $cm^{-3}eV^{-1}$, and rose exponentially towards the valence band. Chew et al. indicated that this value of density of states (DOS) should be taken as the lower limit, because of the difficulty to segregate between the contributions of the interface states of a-SiC and c-Si and the gap states in high-frequency CV measurement. However, in the case of low frequency CV and field effect measurements, the contributions of the interface and gap states can be segrated. Other DOS measurements reported values of 1×10^{16} $cm^{-3}eV^{-1}$ [MATSUURA et al., 1989], 5×10^{15} [MANDEL et al 1994], and 1×10^{17} [SASAKI et al., 1982] from the a-SiC/ c-Si heterostructures. For a-Si film, minima of less than 1×10^{15} $cm^{-3}eV^{-1}$ were obtained by Deep Level Transient Spectroscopy [LANG et al., 1982].

2.5. Applications of a-SiC

The optical and electrical properties of a-SiC films can be tailored by changing the bonding configuration. The defect density in the films could be decreased down to 10^{17} cm^{-3} to achieve a high visible photoluminescence yield of this material at room temperature. These properties, together with other interesting mechanical properties of a-SiC, allow different applications.

2.5.1. Optoelectronic devices

The field of large-area optoelectronic devices benefits considerably from development of the a-SiC thin film deposition technologies and its application in solar cells. These films allowed fabrication of doped and highly transparent entrance windows to single and multijunction solar cells. This has resulted in significant improvements in solar cell conversion efficiencies [KUWANO et al., 1989, SICHANUGRIST et al., 1984, JANG et al., 1997, DENG et al., 2003, JANZ et al., 2006].

The success at bringing down the electroluminescence peak from near IR into the visible region of the spectrum led to applications of a-SiC as a wide gap material to LED devices. The earliest report of EL of a-SiC films at room temperature was made by Munekata et al. [MUNEKATA et al., 1980]. They observed the emission of white light from a simple device and attributed it to the impact ionization of carriers. Later, Kruangam et al. [KRUANGAM et al., 1985, KRUANGAM et al., 1988] described visible light emission from p-i-n type devices. They used the wide band gap a-SiC films as carrier injected layers in a-SiC p-i-n layer LEDs. The EL intensity was augmented by more than 1 order of magnitude by increasing the energy gap of the injector layers, and at the same time the EL spectra shifted toward shorter wavelengths. Other researchers have recently improved the performance of a-SiC thin-film LEDs [SHIN et al., 1993, CHEN et al., 1996]. Lau et al. [LAU et al., 1993] prepared a-SiC thin film LEDs with highly conductive wide gap a-SiC carrier injection layers using PECVD and H_2 dilution. Visible yellowish orange light emissions were observed in these junctions at the room temperature.

Due to the unique property of a-SiC films that the optical band gap can be varied by carbon concentration, color-sensing device have been made using these materials [HAN et al., 1989, MULLER et al., 1995, WIND et al., 1993, KRUTZ et al., 1994]. With band gap varying from 1.7 to 3.4 eV, the region of high monochromatic resolution can be scanned through the entire visible range. Color sensors have been realized with a monochromatic resolution in the blue and ultraviolet region of the visible spectrum.

The a-SiC/c-Si structure has the potential to be useful for Si-based photodetectors. The integration of optics on silicon substrates is expected for applications to optical interconnects or monolithic optical sensors. Photodetectors are important devices for these applications, and have to be fabricated via Si-based processes due to the necessity of the integration on Si substrates [PAUL et al., 1999]. Nishikawa et al. [NISHIKAWA et al., 2006] studied the electrical properties of metal/a-SiC/p-Si structures under various light exposures. a-SiC films were prepared on p-type silicon substrates with resistivities of 5-12 Ωcm by thermal CVD using a monomethylsilane gas as a source gas at 1000 °C. The thickness of the films varied from 5.6 to 43 nm. Tin oxide (SnO_2) electrodes allow the light to pass to the photodetectors. The full width at half maximum (FWHM) of the Si-C peak in FTIR spectrum was equal to that of the poly-crystalline films. However, the RHEED pattern indicated that the SiC film with the thickness of 57.1 nm is amorphous. Nishikawa et al. considered that the SiC film is amorphous or is close to being poly-crystalline. From IV characteristics, it was observed that at positive voltages (reverse bias), the current densities were nearly equal for different thicknesses. However, they observed the difference between the photo and dark current densities at positive voltages. They indicated that the Al/a-SiC/p-Si structure operates as a photodetector at reverse bias. The difference between the photo and dark current densities was proportional to the light intensity when they measured the current with changing the light intensity. Their a-SiC was assumed to be intrinsic (its resistivity was higher than 9×10^2 Ωcm) and had a band gap energy of 2.2 eV. They explained the conduction mechanism of the dark current by thermionic emission. For the electron current, the current is given by the concentration of electrons with energies sufficient to overcome the energy difference between the bottom of the conduction band of the SiC and the Fermi energy of the Si. The

sum of the Fermi energy and the energy difference is the minimum energy required for thermionic emission from the Si into the SiC. At positive voltages, the dominant current is considered to be the electron current from Si to the metal, because the energy difference of electrons at the SiC/p-Si interface is lower than the barrier height of holes at the Al/SiC interface. At negative voltages, the dark current is considered to be the electron current from the metal to Si and the hole current from Si to the metal. The dark current at positive voltages is lower than that at negative voltages because the energy difference of electrons at a-SiC/p-Si interface under positive voltages is higher than the barrier height of electrons at the Al/SiC interface or the energy difference of holes at the SiC under negative voltages. Under light exposure, they proposed that the electron-hole pair generation in p-Si is due to the absorption of photons with energies grater than the silicon band. The photo-generated electrons reach the SiC/p-Si interface resulting in an increase in the current.

2.5.2. Passivation Layers

Surface passivation is an important step in advanced solar cell technology. Amorphous based layers like SiN_x, SiO_x and a-Si have been already applied in numerous Si-based solar cell applications. They are used as diffusion barriers, anti-reflection coatings, surface passivation layers, or as a hydrogen source to passivate the silicon bulk material. The only observed drawbacks are their relatively poor thermal stability and their lack of conductivity (electrical and thermal). However, a passivation layer must keep its passivating properties after the final thermal step. In addition, the deposition process must be fast enough such that manufacturing cost does not increase. a-SiC thin films with low conductivity ($\sigma \approx 10^{-9}$ Scm^{-1}) and wide energy gap, show properties similar to other dielectric materials mentioned above. Therefore, many efforts have been made to introduce a simpler surface passivation consisting of a single layer of a-SiC with better characteristics. Among them Martin et al. [MARTIN et al., 2001] have investigated a surface passivation of p-type crystalline Si by plasma enhanced chemical vapor deposited a-SiC films. A 70 nm-thick a-SiC layer was deposited on a cleaned surface of p-Si wafer with a resistivity of 3.3 Ωcm. The optical band gap of a-SiC ranged from 1.8 to 2.2 eV. A surface recombination velocity lower than 30 cm s^{-1} was measured by quasi-steady-state photoconductance. By comparing these results with those of a-Si films it

was concluded that carbon incorporation does improve the passivation properties of these films. Janz et al. [JANZ et al., 2006] reported an overview of the activities to investigating SiC as an alternative to SiN_x and SiO_x. a-SiC layers were prepared by PECVD, at 350 and 550 °C. FTIR showed that the hydrogen related bonds have been broken at annealing temperatures up to 950 °C, and led to hydrogen effusion and formation of new Si-C bonds. With increasing the annealing temperature, the onset of a crystallization process was observed by X-ray diffraction (XRD) measurements. They prepared a-SiC with different band gap energies ranging from 2.0 to 2.4 eV by changing the gas flow ratio, which also resulted in changing the refractive index from 3.6 to 2.3. Since the transition metals significantly increase the minority carrier recombination rate, a-SiC is used as an electrically conductive diffusion barrier layer in Si thin-film solar cells. Janz et al. calculated the diffusion constants for iron (at 1200 °C) of 3×10^{-15} to 4×10^{-16} cm^2S^{-1} for the stoichiometric SiC layers. These value are comparable to the value of other plasma deposited layers like SiO_2 (7×10^{-13} cm^2S^{-1}) or SiN_x (3×10^{-14} cm^2S^{-1}). Lifetimes of >1500 μS on SiC passivated silicon wafers were measured using quasi steady state photoconductance method. It was concluded that the a-SiC material has the potential to combine features like diffusion barrier performance, tuneable band gap, conductivity, source for hydrogen, surface passivation, thermal stability, stress tuning and a relatively flat quantum well for a better carrier transport in quantum dot super lattices.

2.5.3. Coating material

High-reflectance amorphous silicon carbide films have been used to coat figured glass and metal for ultraviolet optics [LANG et al., 1993, KORTRIGHT et al., 1988]. By fabricating a concave replica diffraction grating coated with a-SiC material, Kortright et al. demonstrated the improved ultraviolet performance of the a-SiC films. The grating showed absolute diffraction efficiencies on the order of 20% near normal incidence in the spectral region from ~800 to 1200 Å.

Other recent application of a-SiC are summarized as follows:

- As the high-resistance spacer layer in gas avalanche pixel detectors [KORTRIGHT et al., 1988, CHO et al., 1996, HONG et al., 1998]
- As undoped cladding layers in planar-guided wave structure [SHEN et al., 1995, COCORULLO et al., 1996, AMATO et al., 1993]
- In a-SiC/a-Si metal base transistor [SZE et al., 1966, JWO et al., 1986, JWO et al., 1988]
- As an electron photoinjecting electrode in spatially addressable light transducer [MULLER, 1997, HIRAMOTO et al., 1990]

CHAPTER 3: AMORPHOUS MATERIALS

In a crystal, the atoms or molecules are arranged in a regular structure and the lattice periodicity can extend over a distance of centimetres with remarkably few structural defects (see figure 3-1a). In an amorphous solid there is no long-range ordered structure, although the basic properties of the chemical bonds that bind the solid together define a certain amount of short-range order. The short-range order merely extends over a few atomic spacing, that is, over a distance of about 1 nm from any given atom. In an amorphous solid, the periodic structure of the crystal is replaced by a random network of atoms or molecules (see figure 3-1b). This difference in the atomic arrangement in the crystalline and amorphous phase can influence many of the properties of the material [MILLER et al., 1991]. The most important difference between a crystalline and amorphous semiconductor is the continuous distribution of localized states within the forbidden energy gap in the amorphous material. These states arise from the defects of the material with respect to the perfect crystal and their density depends critically on the method used to prepare the amorphous film.

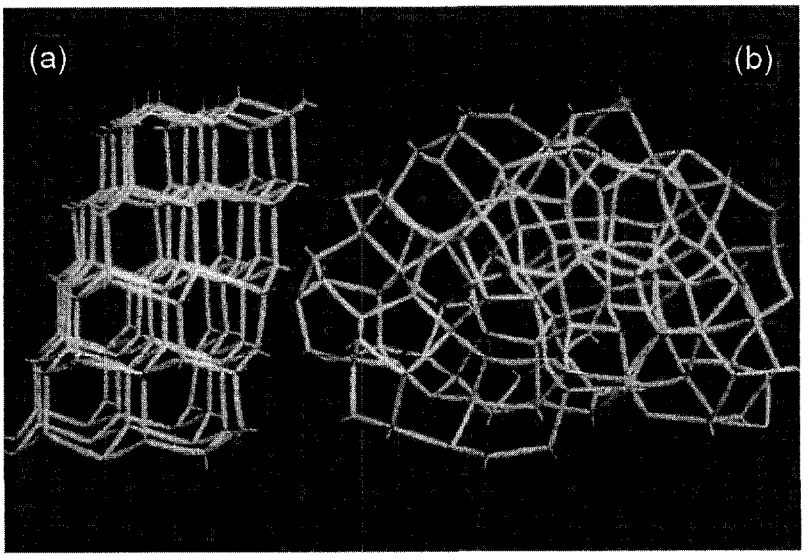

Figure 3-1 Models illustrating the structure of (a) crystalline and (b) amorphous materials [MILLER et al., 1991]

Another important difference between amorphous and crystalline materials concerns the mobility of the electrons or holes. In a crystal, an electron or hole in the extended band states can move many atomic distances before it is scattered by something that perturbs the periodicity of the lattice. In an amorphous material the periodicity of the lattice only extends over a few atomic spacing. Under these conditions the electron transport may no longer be considered as band motion with occasional scattering. In this case, the electron motion is essentially a diffusive process which can be considered similar to the Brownian motion of small particles in liquids. The definition of mobility and its dependence on the other properties of material will be presented in section 3.1. In section 3.2, it will be explained how the amorphous interlayer could be applied in contact barrier devices to modify characteristics such as barrier height and leakage current. Some properties of the amorphous layers could be extracted using heterojunction devices which will be also discussed in section 3.2.

3.1. Mobility of charge carriers in amorphous materials

The mobility (μ) is usually defined macroscopically, as the proportionality factor between carrier drift velocity v_d and the applied electric field E at low field ($v_d = \mu E$). From a microscopic point of view, carrier mobility is determined by the scattering phenomena which a carrier experiences during its motion under the action of the electrical field E. Hence, a higher mobility material is likely to have a higher frequency response. The device current depends on the mobility so the higher mobility materials have higher current. Higher currents charge capacitances more rapidly, resulting in a higher frequency response.

Mobility varies with temperature, and its value decreases with the effective mass, (m^*). Also, as the impurity concentration augments the mobility reduces.

It should be noted that there are several kinds of mobility corresponding to the determination method used [SCHRODER, 1990]:

- Microscopic mobility is calculated from basic concepts and describes the mobility of the carriers in their respective band.

- Conductivity mobility concerns the conductivity or resistivity of a semiconductor material. To determine the conductivity mobility, it is necessary to measure the majority carrier concentration and either the conductivity or the resistivity of the sample independently. The mobility of electron and holes are given by:

$$\mu_n = \sigma / qn \tag{3-1}$$

$$\mu_p = \sigma / qp \tag{3-2}$$

Where n and p are the carrier density of electron and holes, respectively, and q is the electronic charge.

- Hall mobility is determined from the Hall effect and differs from the conductivity mobility by a factor that depends on the scattering mechanism (r) ($\mu_H = r\mu_n, \mu_H = r\mu_p$). The factor r is larger than unity. For most Hall determined mobility, r is taken as unity, but this assumption should be carefully specified.

- Drift mobility is the mobility measured when minority carriers drift in an electric field. It is device-oriented mobility. The minority carrier mobility would be lower than the majority carrier mobility, if carrier-carrier scattering is significant compared to the lattice and ionized impurity scattering.

- The geometry has a major influence on the mobility in some devices, so the resulting mobility, determined from the device current-voltage characteristic, is named the effective mobility (μ_{eff}).

The basic transport properties usually measured in semiconductors are the conductivity σ and the Hall coefficient R_H [BRODSKY, 1985]. For unipolar conduction, measurements of the Hall coefficient provide a reliable guide to the charge carrier concentration. For n-type semiconductors the Hall coefficient is negative and is given by the general formula,

$$R_H = -\frac{r}{ne} \tag{2-3}$$

Here r is the scattering factor and is usually not much greater than one. In p-type semiconductors, the Hall coefficient is positive. From σ and R_H we may determine the Hall mobility:

$$\mu_H = |R_H|\sigma = r\mu \tag{3-4}$$

Thus the Hall mobility is greater than the conductivity mobility by the scattering factor r. Interpretation of the Hall coefficient on this basis is valid for materials in which the mean free path is long compared to the interatomic spacing. In amorphous semiconductors the mobilities are found to be very low so the carriers will move with a mean free path comparable to the interatomic distance. As a consequence, the ordinary transport theory based on the Boltzmann equation cannot be used anymore. So far, the measurements of the Hall coefficient have been made for a limited number of amorphous semiconductors, due to the limitations imposed by the high resistivity and the low carrier mobility of the material. The sign of the Hall effect measured on the amorphous material has been reported to be electron-like (negative) for p-type doping and hole-like (positive) for n-type doping and intrinsic material [NEBEL et al., 1993].

3.2. Application of amorphous materials in contact barrier diode

Devices employing amorphous materials have received considerable attention in last two decades due to the numerous advantages of these materials. Metal-semiconductor rectifying junctions (Schottky barriers) have been traditionally used for both materials' characterization and in device structures [RHODERICK et al., 1988]. Fabrication of ideal Schottky contacts on III-V semiconductors is difficult, due to the Fermi level pinning phenomenon, which leads to a low barrier height, thus limiting applicability. The problem of low barrier height and high leakage currents can be overcome by modifying the semiconductor surface using thin interfacial layers. The interfacial layer can be an insulator, a large band gap crystalline

semiconductor, or an amorphous semiconductor. The latter presents many advantages compared to the other two layers, and hence seems to be the best alternative.

3.2.1. Role of the amorphous interlayer

It is known [KANICKI, 1991] that in the metal/amorphous layer/III-V semiconductor diodes, a barrier appears at the semiconductor surface, in series with the barrier at the metal/amorphous layer interface and with the effective resistance of the amorphous layer. If the amorphous interfacial layers are very thin, the electrons will have a high probability of tunnelling through the amorphous layer, possibly via localized states in the amorphous layer. In this case, the barrier at the semiconductor surface will dominate the current transport through the diode. The maximum thickness for this tunnelling to become significant depends on the metallization, because of the variations in the extent of the reactions and of the interdiffusion at the metal/amorphous layer interface. For thicker layers, the reverse and low forward-bias current will be controlled by the higher of the two barriers present, whereas at higher forward bias, the effective resistance of the amorphous layer will control the diode current. As a consequence of its high resistivity, a thin layer of amorphous material injected with a charge gives rise to a transition to space-charge-limited current (SCLC) I proportional to V^m behaviour with $m>1$. The dominant conduction mechanism is SCLC, when sufficient carriers are injected into a thin insulator or semiconductor so that the resulting space charge from the injecting contact extends across the entire sample width [YABE et al., 1984]. The current flow may then significantly exceed the ohmic current. The actual relationship between the current and voltage is dependent on the distribution of traps in the sample.

3.2.2. Capacitance-voltage characteristics

Capacitance-voltage (CV) characteristics vary with the measuring frequency, because of the dielectric relaxation and of the traping/detrapping processes in the amorphous film. It is easy to measure high-frequency (e.g., 1 MHz) CV characteristics [MATSUURA, 1988, SASAKI et al.,, 1982a, SASAKI et al., 1982b, SZE, 19981]. When the measuring frequency is high enough, the dielectric relaxation process, as well as the trapping/detrapping process in the

amorphous film can be neglected. Thus, the change in the width of the depletion region in the crystalline semiconductor, produced by the dc reverse bias, is the only factor needed in order to calculate the capacitance. The contribution of the amorphous layer to the measured capacitance is equal to the geometric capacitance of the amorphous film due to its longer dielectric relaxation time, whereas that of crystalline semiconductor is associated with the depletion width (W). The measured capacitance (C_T) is essentially the result of two capacitances in series; the amorphous layer capacitance, $C_a = k_a A/d$ and the crystalline semiconductor space-charge capacitance $C_c=k_c A/W$. Here, A is the area of diode, d is the thickness of amorphous layer, and k_a and k_c are the permittivity of amorphous and crystalline layers, respectively.

$$C_T = C_a C_c (C_a + C_c)^{-1} = A k_a k_c (k_a W + k_c d)^{-1} \tag{3-5}$$

$$W = \left[\frac{2k_a (V_{bi} - V + kT/q)}{q|N_A - N_D|} \right]^{1/2} \tag{3-6}$$

Where $N_A(N_D)$ is the concentration of acceptors (donors) in the crystalline semiconductor, and V_{bi} is the built in voltage.

Figure 3-2 shows the typical high-frequency (1 MHz) CV characteristics of the undoped a-Si:H/p c-Si ($N_A=10^{16}cm^{-3}$) heterojunction. The capacitance is nearly independent of the applied voltage [MATSUURA, 1989]. The value of this capacitance is determined by the film thickness of amorphous layer. This capacitance could be used to approximately ($k_a = C_a d/A$) calculate the permittivity of the amorphous layer. In the intrinsic amorphous layer, the thermal emission rates of electrons from the localized states to the conduction band are usually much lower than the capture rates of electrons from the conduction band into the localized states, therefore the capacitance should be measured from a higher to a lower reverse bias. Moreover, the voltage sweep rate (dV/dt) should be small, for example dV/dt should be smaller than 0.004 V/s, and the heterojunction at higher reverse bias (starting bias for the CV measurements) should be kept for a few minutes in order to get the steady-state condition [[KANICKI, 1991].

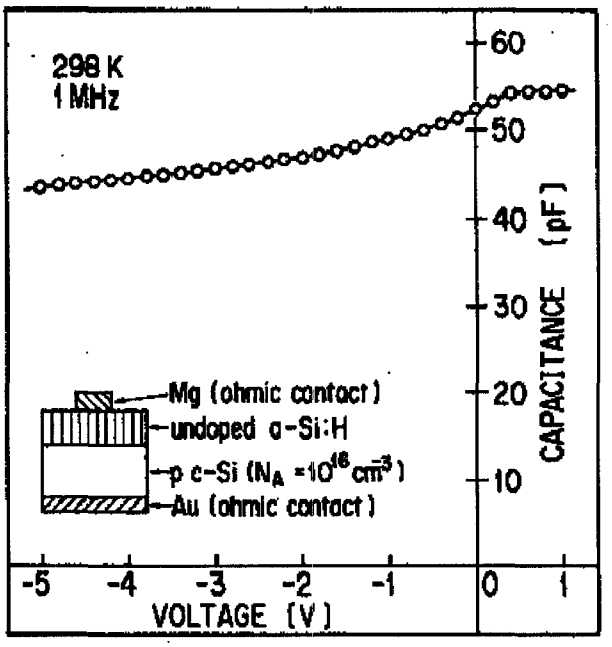

Figure 3-2 Room temperature capacitance voltage characteristics of undoped a-Si:H/p-c-Si ($N_A = 10^{16}\ cm^{-3}$) heterojunction [MATSUURA, 1989]

3.2.3. Current-voltage characteristics

Figure 3-3 shows the typical current-voltage (*IV*) characteristic in semilog presentation for the undoped a-Si/p-c-Si heterojunction. Two current transport mechanisms are proposed to explain this *IV* characteristic [MATSUURA, 1988].

1. A bulk-limited (space-charge-limited) transport mechanism.
2. A junction-limited current transport mechanism.

The essential difference between (1) and (2) is whether the resistance of the depletion region is greater or smaller than the resistance of the amorphous film. In the bulk-limited case the applied bias drop is mainly across the amorphous layer; in the junction-limited case the applied bias drop is across the depletion region.

Injection of charge carriers into a high resistive interfacial layer results in a gradual transition from ohmic ($I \propto V$) to space charge limited current (SCLC) ($I \propto V^m$) characteristics with an increase in forward bias [DUTTA et al., 1995]. At low potentials, as shown in figure 3-3, the *IV* characteristics are barrier-dominated, but in the high voltage regime, strong injection of excess carriers occurs and the quasi-Fermi level moves through an appreciable energy range towards the corresponding band. The effect of SCLC decreases the effective series resistance above a certain threshold voltage, drastically leading to rapid increase in the current.

A comparison of the *IV* characteristics of the Schottky diode with and without an amorphous interfacial layer shows an augmentation in the turn-on voltage after the application of the interfacial layer. The turn-on voltage increases further with an increase in the film thickness. In the reverse bias region, the diodes with an interfacial layer exhibit a lower reverse current, and higher breakdown voltage [DUTTA et al., 1995].

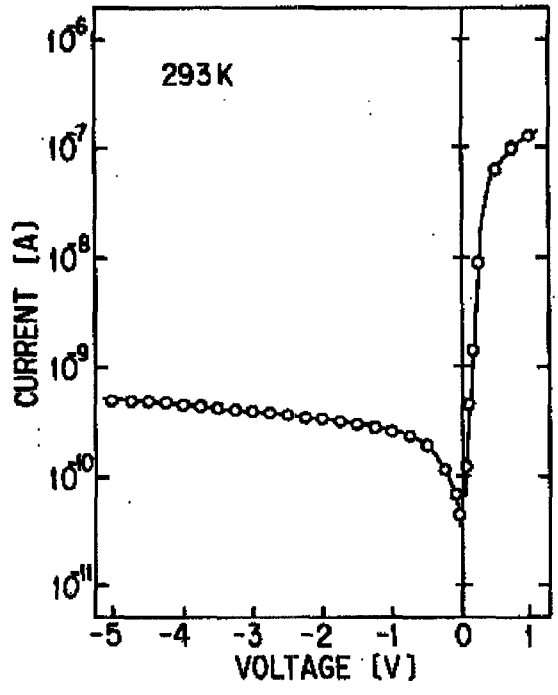

Figure 3-3 Current-voltage characteristics of undoped a-Si:H/p-c-Si ($N_A = 10^{16}\ cm^{-3}$) heterojunction [MATSUURA, 1988]

A theory consistent with a contact barrier diode applying a high resistive interfacial layer is developed as follows [Forrest et al., 1984, Buget et al., 1967]: the current densities for electrons (J_n) and holes (J_p) everywhere in the device are given by

$$J_n = q\mu_n nE \tag{3-7}$$

$$J_p = q\mu_p pE \tag{3-8}$$

With the total current given by $J=J_n+J_p$. Here q is the electronic charge, μ_n (μ_p) is the mobility of electrons (holes), and E is the electric field. Also, the carrier densities (n,p) are the sum of the equilibrium (n_0,p_0) and injected (n_{inj},p_{inj}) densities. In the following discussion, the considered carriers are holes, although similar expressions can be written for electrons. Thus,

$$P = P_0 + P_{inj} = N_v \exp\left[E_v - \psi_p)/kT\right] \tag{3-9}$$

where N_v is the density of states at the valence band edge ($\in_v$), kT is the Boltzmann energy, and ψ_p is the quasi-Fermi energy for holes.

Since the conductivity of the interfacial layer is very low, p_0 in this material is small, the Fermi energy is in most cases determined by the density of injected charges, and the transport within the material is space-charge limited.

From current continuity:

$$\frac{dJ}{dx} = \frac{dJ_n}{dx} = \frac{dJ_p}{dx} = 0 \tag{3-10}$$

which is valid at all points within the diode in the absence of charge recombination. From Eq. (3-7), (3-8), and (3-10), and using Poisson's Equation, it can be shown that the electric field in the space-charge layer is

$$E_{Sc}(x) = \left[\frac{-2J_x(\xi - 1)}{k_a(\mu_p + \mu_n)}\right]^{1/2} \tag{3-11}$$

Where $\xi = n/p << 1$, $\xi \approx 0$, and k_a is the permittivity of interfacial layer. From Eq. (3-11), $E_{sc}=0$ at the surface of interfacial layer ($x=0$). Using $E=-dV/dx$ and setting $x=d$, the current density in the film with thickness d could be expressed by the Mott-Gurney relation:

$$J = (9/8)\frac{k_a \mu_p V_{Sc}^{\ 2}}{d^3} \tag{3-12}$$

where V_{sc} is the voltage drop across the space-charge region.

When contact is made between interfacial layer and crystalline substrate, the hole current is limited by thermionic emission over the barrier of height ϕ_{Bp}. Under reverse bias, the saturation current in the organic layer (J_s) is given by:

$$J_s = -A^* T^2 \exp\left[-q(\phi_{Bp} - \Delta\phi)/kT\right] \tag{3-13}$$

Here, A^* is the Richardson constant, $\Delta\phi$ is the image force barrier lowering given by $\Delta\phi = \sqrt{qE_m / 4\pi k_c}$, k_c is the permittivity of the crystalline substrate, and E_m is the electric field in the substrate at $x = d$.

Requiring the continuity of both hole and electron currents leads to the familiar expression for thermionic emission across the contact barrier diode:

$$-J = J_s\{\exp[-q(V_a - V_{sc} - V_R)/nkT] - 1\} \tag{3-14}$$

where n is the diode ideality factor and V_a is the applied voltage such that

$$V_a = V_D + V_{sc} + V_R \tag{3-15}$$

In the equation above, V_D is the voltage drop across the crystalline semiconductor and V_R is the total voltage across the device series resistances (R). Thus

$$J = V_R / (RA) \tag{3-16}$$

The thermionic emission SCLC model implies that high electric fields are developed in the crystalline substrate at low current densities, whereas at high currents, the highest fields are in the interfacial thin film. The maximum field in the substrate will be at its surface (x=d) and is given by:

$$E_m = 2V_D / W \tag{3-17}$$

And the maximum field in the amorphous layer is estimated using equation (3-11):

$$E_{sc} = \left(\frac{2dJ}{k_a \mu_p} \right)^{1/2} \tag{3-18}$$

In the preceding discussion, the effect of diffusion and charge trapping on the interfacial layer were neglected. However, traps play an important role in the current transport in amorphous material. It has been shown [Rose, 1963] that the space-charge current in the presence of traps is given by

$$J = (9/8) k_a \mu_{eff} V_{sc}^2 / d^3, \tag{3-19}$$

where the effective mobility is $\mu_{\text{eff}} = \theta \mu_{\text{p}}$. Here,

$$\theta = p / p_T < 1 \tag{3-20}$$

where p_T is the number of trapped holes. The filling of traps reduces the electric field at the interface, which in turn reduces the space-charge-current. The transit time of carriers across the space-charge layer can be estimated using

$$\tau \approx \frac{d^2}{\mu_{eff} V_{sc}} \tag{3-20}$$

This indicates that τ increases with decreasing V_{sc}.

CHAPTER 4: EXPERIMENTAL DETAILS

4.1. Preparation of a-SiC

Amorphous SiC thin films were deposited by PSCVD method, using 0.3 g of solid poly dimethylsilane at 1300-2700 Pa above the atmospheric pressure. The details of the PSCVD method have been already reported elsewhere [SCARLETE et al., 2003]. a-SiC films were obtained in few minutes, at maximum deposition-rates of over 250 Å/min. Four sets of samples were produced at temperatures of 750 °C, 850 °C, 950 °C and 1000 °C. Faster deposition rates have been obtained at higher temperatures, while the yield of the deposition has not been significantly affected by the temperature. The substrates used were <100>-oriented, n- and p-type silicon single crystal wafers with resistivity in the range of 1-10 Ωcm and 1 μm silicon dioxide thermally grown on Si single crystal wafers. The deposition temperature, substrate and thickness of each sample are presented in Table 4-1.

TABLE 4-1 DEPOSITION CONDITIONS FOR A-SIC THIN FILMS

Sample No.	Substrate	Dep. Temp. (°C)	Thickness (nm)
1	n-Si	750	200
2	p-Si	750	250
3	SiO_2	750	200
4	n-Si	850	250
5	p-Si	850	251
6	SiO_2	850	260
7	n-Si	950	100
8	p-Si	950	42
9	SiO_2	950	220
10	n-Si	1000	40
11	p-Si	1000	210
12	SiO_2	1000	500

4.2. Characterization methods

Thin films of a-SiC prepared using PS-CVD method were the subject of different tests. First the chemical characterization was done to examine the composition and atomic concentration of different elements in this material. The Fourier-transform infrared (FT-IR) spectroscopy analysis provided valuable information on the composition of the deposited films. FT-IR measurements were performed using a Galaxy 6020 series infrared spectrometer from Mattson Instruments at Bishop's University. The spectra were recorded in the 400 to 4000 cm^{-1} wave number range (mid-IR), with a resolution of 4 cm^{-1}.

The atomic concentrations of all significant chemical elements were determined by ERD analysis, using the upgraded EN-1 HVEC Tandem accelerator. Details of the ERD method are explained in section 4.2.1.

CV measurements were applied to all samples, using the 1260 Schlumberger instrument. The measurements were done at 1 MHz small signal with amplitude of 15 mV, which was superimposed to the bias voltage. The device considered was a Schottky diode, achieved with mercury probe contacts placed on surface of the deposited film.

The ohmic contacts consisted of 150 nm nickel dots with the area of 7.85×10^{-3} cm^2 separated by 0.5 cm, deposited on a-SiC, followed by a rapid thermal annealing (RTA) process at 800 °C for 2 minutes. The contacts have been tested by applying IV measurements using HP4145A semiconductor parameter analyzer.

The Hall effect measurements were performed for the samples which were deposited at 1000 °C on insulating substrates. A detail of the measurement technique is presented in section 4.2.2. This type of measurement was not possible for the thin films deposited at low temperatures due to their high resistivity as it was already explained in section 2.2. The thin films of a-SiC, which were deposited at low temperature (750 °C), were considered as interfacial layers in three samples of contact barrier diode. IV and CV characteristics of these devices were used to determine some properties of a-SiC layer such as dielectric constant,

mobility and lifetime. For these devices, aluminium was evaporated at broad back side of silicon as the back ohmic contact.

4.2.1. ERD measurements

The composition depth profile of the films was determined using ERD-TOF (Elastic Recoil Detection Time-of-Flight) [Gujrathi et al., 1996, Schiettekatte et al., 2004] facility of Université de Montréal. Briefly, in ERD-TOF technique, atoms of the constituent elements are ejected from the sample in the forward direction by a high energy heavy ion beam. The recoiled atoms and the probing scattered ions (when the scattering angle is less than certain critical angle) pass through a thin carbon foil (5-10 $\mu g/cm^2$) generating first timing signal. After traveling a short flight path they are stopped in a cooled (-10 °C) silicon surface barrier detector creating both energy and second timing signals. The flight time and the energy information allow mass identification while the number of counts is related to the concentration. The second surface barrier detector with range foil enables H depth profiling simultaneously.

In the present investigations the probing beam was $^{59}Co^{8+}$ ions accelerated to 40 MeV, making equal entrance and exit angles with the target surface resulting in a scattering angle of 30°. To analyze the film composition underneath the Ni contact, the beam was collimated to a small size which produced a spot of 0.6 x 0.6 mm^2 on the sample in the 30° scattering geometry. The film compositions very near to the Ni spots were also studied by shifting the sample positions. Several Ni contact diode structures were studied.

4.2.2. Hall measurements

The key feature of Hall measurements is the ability to determine the carrier concentration, the carrier type, the resistivity, and the mobility with a relatively simple measurement.
As originally devised by van der Pauw [Pauw, 1958a, Pauw, 1958b] we can use an arbitrary shape with four ohmic contacts as shown in figure 4-2.

- The contacts are at the circumference of the sample.

- The contacts are sufficiently small.
- The sample thickness is uniform.
- The sample surface is singly connected. (i.e., the sample does not contain isolated holes.)

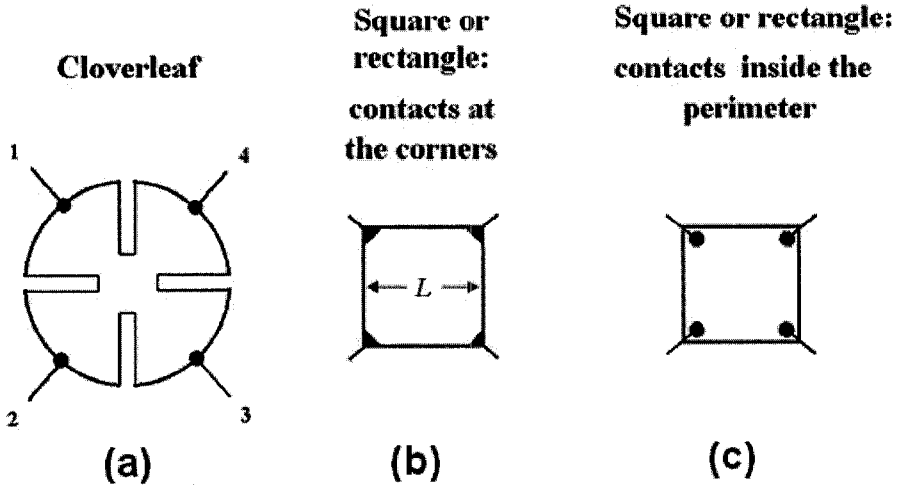

Figure 4-1 The arbitrary shaped samples for Hall measurements: (a) , (b) acceptable to determine the carrier concentration, carrier type, resistivity, and mobility, (c) recommended only for mobility measurement [Pauw, 1958a]

The following equipment is required for Hall measurement using van der Pauw's method:

1. An electromagnet, (500-5000 G, measurement in low field limit: B<<10 kG).
2. Constant-current source with current ranging from 10 μA to100 mA.
3. A high input impedance voltmeter covering 1 μV to 1V.

Preparing the sample:

A metallic masque which has the holes at a distance of 5 mm and the diameter of 1 mm was used for deposition of 200 nm Ni. The contacts were annealed at 800 °C for 2 min. The samples were cut in square pieces as needed by the van der Pauw technique.

The contacts were tested by applying the IV measurements before and after annealing. A preliminary determination of contact resistances is necessary for establishing the suitable current source. A DC current was adjusted on the current source for further application to the

sample. Conditionally, the power dissipation should not exceed 5 mW (preferably 1 mW). This limit can be specified before starting the measurement by calculating the resistance R between any two opposing leads (1 to 3 or 2 to 4) and setting $I < (200R)^{-0.5}$.

Four leads (micro-fills) were connected to the four ohmic contacts on the sample. The sample was placed in a ferric box which made the cables' connection possible. An interface box was used for changing the positions of the input current and of the output voltage.

The measurement sequences have been set as it follows:

1. Set a DC suitable current
2. Set the voltmeter limiting voltage at 10 V
3. Put the interface box at the first position, apply the current and read the voltage. (V_1)
4. Switch to the positions 2, 3, and 4, repeat step 3. (V_2, V_3, V_4)
5. Change to the position by 5, apply the current, and turn on the magnetic field (the current at electromagnet should be set at 12 A for having a magnetic field at 1.2 kG), read the voltage (V_{5a}), turn off the magnetic field and read the voltage (V_{5b}).
6. Change to the position by 6, repeat step 5. (V_{6a}, V_{6b})

The following calculations must be done to determine the Hall mobility from the measured values:

$$V_5 = V_{5a} - V_{5b}$$

$$V_6 = V_{6a} - V_{6b}$$

$$V_H = (V_5 + V_6)/2$$

$$V_{34} = (V_1 + V_3)/2$$

$$V_{41} = (V_2 + V_4)/2$$

$$R_{12,34} = V_{34} / I$$

$$R_{23,41} = V_{41} / I$$

$$\rho = (\pi.t / ln2).(R_{12,34} + R_{23,41}).F / 2$$

$$R_H = t.V_H / B.I$$

$$\mu_H = |R_H| / \rho$$

$$n = 1/(q.\ R_H)$$

Where $F = 1$ for symmetrical samples and d is thickness of the sample.

These testes were done for a set of the a-SiC samples suitable prepared for Hall measurements. The results will be discussed in the next chapter.

CHAPTER 5: MATERIAL CHARACTERIZATION AND DISCUSSION

The chemical characterizations of deposited a-SiC thin films were done using FT-IR spectroscopy and ERD techniques, while the CV characterization technique gave the information about conductivity of this material. The contact characteristics of prepared a-SiC thin films were studied using IV measurements before and after annealing. The contacted material was subjected to the Hall effect measurements using van der Pauw technique. The results of FT-IR and ERD characterisation together with the results of CV measurements will be discussed in the first section. The characteristics of Ni contacts deposited on a-SiC thin films will be presented and discussed in second section and the result of mobility measurements will be found in the last section of this chapter.

5.1. Material characterization

Figure 5-1 shows the IR absorption spectra of the films deposited at various temperatures on (a) n-type silicon and (b) p-type silicon. Similarity of figure 5-1(a) and 5-1(b) indicate that the substrate has no appreciable effect on the film composition. However, comparison between the films deposited at different temperatures clearly indicates a change in the structure and in the composition of the film.

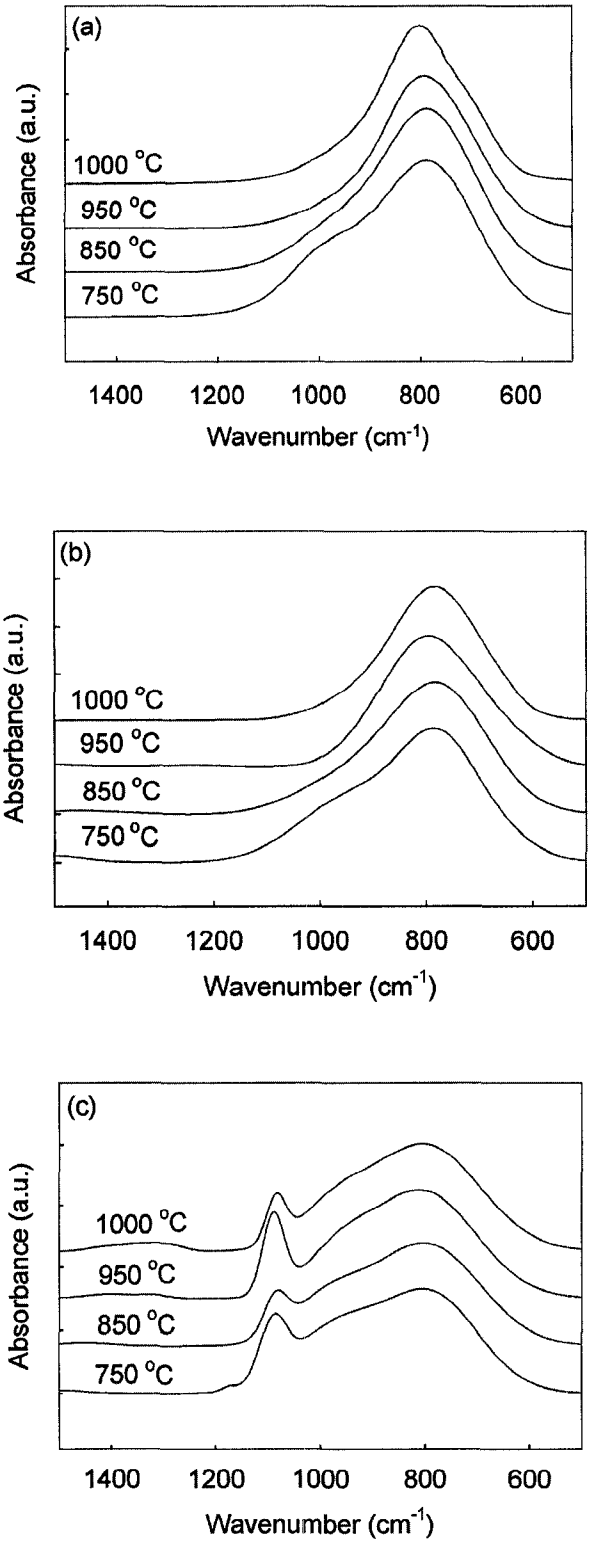

Figure 5-1 FT-IR spectra in the 500-1500 cm^{-1} region of thin film deposited at temperatures of 750, 850, 950 and 1000 °C on (a) n-type silicon substrate, (b) p-type silicon substrate, and (c) silicon dioxide thermally grown on silicon substrate

As it is seen in figure 5-1 the main absorption band located at around 795 cm^{-1} is attributed to SiC formation [Zhuge et al., 2004a]. However, the shoulder at 1000 cm^{-1} is assigned to the wagging mode of Si-CH_2-Si [SCARLETE et al., 1995, Kaneko et al., 2005, Tabata et al., 2003, Zhang et al., 2004b] groups, and therefore is correlated with the amount of residual hydrogen. The latter decreases considerably for the samples deposited at higher temperatures. The samples deposited at 1000 °C on the silicon substrates show a more symmetrical and a sharper absorption band situated at 795 cm^{-1}. The full width at half maximum (FWHM) of the peaks are gradually reduced by increasing the deposition temperatures. The general narrowing of the bands demonstrates that the films are becoming structurally more ordered, *via* increased size of the initial grains [Kaneko et al., 2005].

Figure 5-1(c) presents the FT-IR spectra of the thin films deposited on the silicon dioxide substrates. In all spectra, the maximum of the main absorption band is located at about 810 cm^{-1}. The broadness of this absorption is the result of the overlap of many constituent bands, such as Si-C at 795 cm^{-1} and Si-O bending at 810-820 cm^{-1} [Kaneko et al., 2005, Mahajan et al., 2004], Si-OH at 950 cm^{-1} [Fu et al., 2003] and Si-O asymmetric stretching mode of silicon dioxide at 1080 cm^{-1}, which are overlapped by the separate band linked to the interstitial oxygen in the substrate centered at 1100 cm^{-1}. As observed in figure 5-2, the ERD measurements show a constant concentration of oxygen in the films deposited on all substrates. The presence of oxygen at the interface of Si and a-SiC in figure 5-2(a), 5-2(b) is due to the native oxide on the surface of silicon.

Figure 5-3 shows the oxygen concentration in the films deposited on SiO_2 substrates at different deposition temperatures. It is observed that with increasing deposition temperature, the concentration of oxygen in these film decreases. The sudden decrease of the oxygen concentration from 65% to 8% indicates the location of the interface between the SiO_2 substrate and the deposited a-SiC.

The hydrogen concentration in the films was also compared for the a-SiC thin films deposited on SiO_2 substrate at different deposition temperatures. The result is shown in figure 5-4. It is seen that the concentration of oxygen in the films decreases by increasing the

deposition temperature, which was also indicated using the IR absorption spectra in figure 5.3.

The high hydrogen concentration in the thin film of a-SiC deposited at 750 ^{o}C indicates that this film could be a promising candidate for crystalline semiconductor surface passivation. The employing of hydrogen induces additional charge of positive sign on the semiconductor side of the interface and results to the increasing or decreasing of the barrier heights.

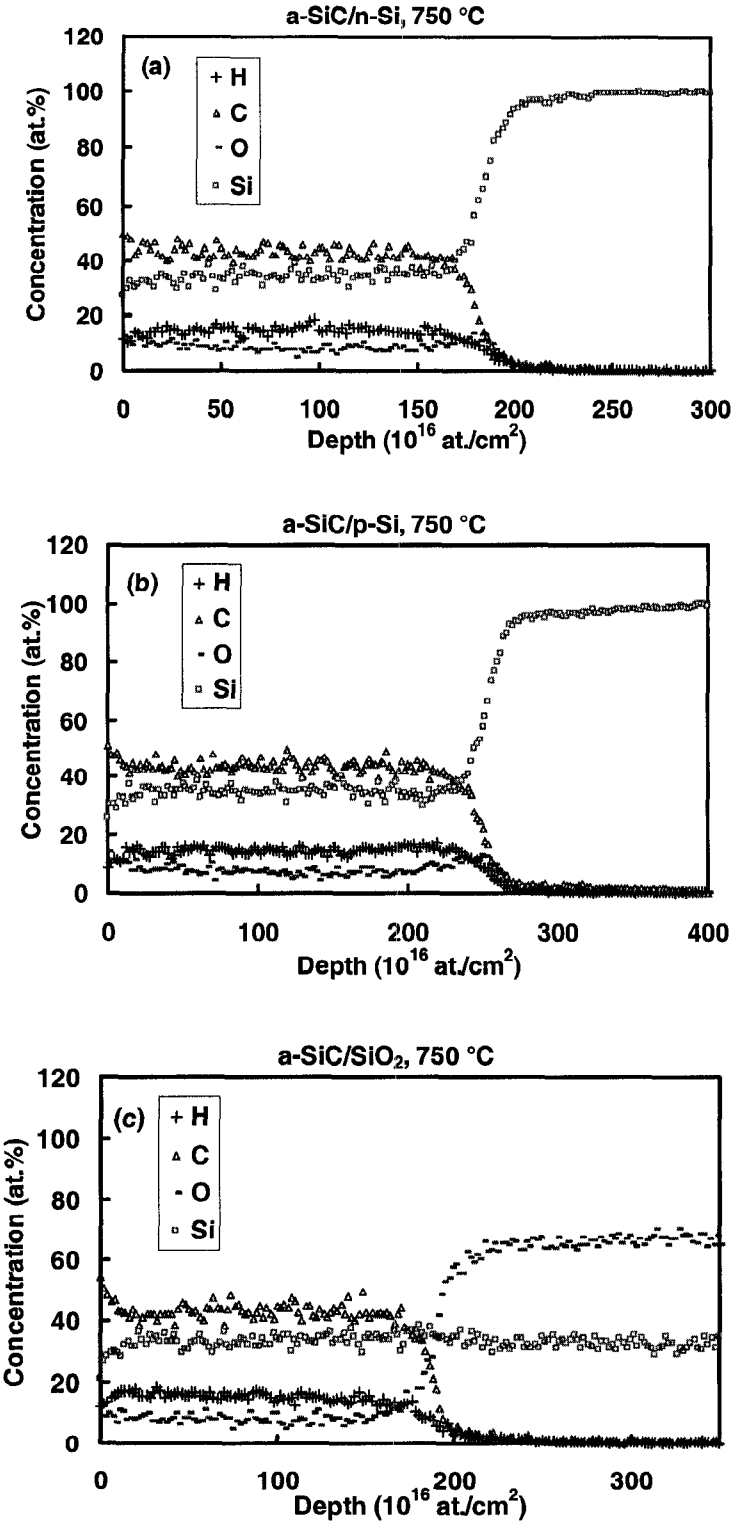

Figure 5-2 ERD measurement of thin film deposited at 750 °C on (a) n-type silicon substrate, (b) p-type silicon substrate, and (c) silicon dioxide thermally grown on silicon substrate

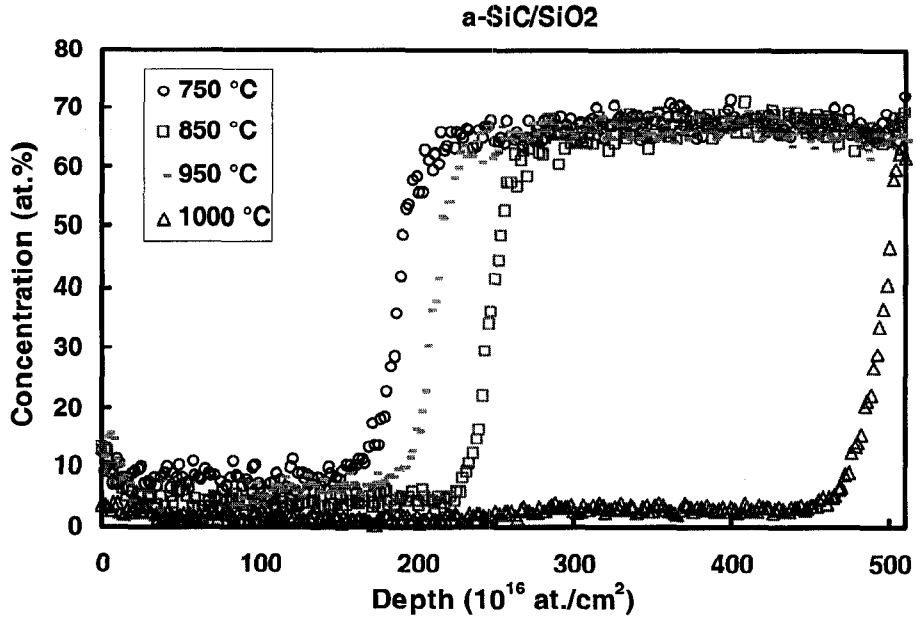

Figure 5-3 Oxygen concentration in the films deposited at temperatures of 750, 850, 950 and 1000 °C on SiO_2 substrate

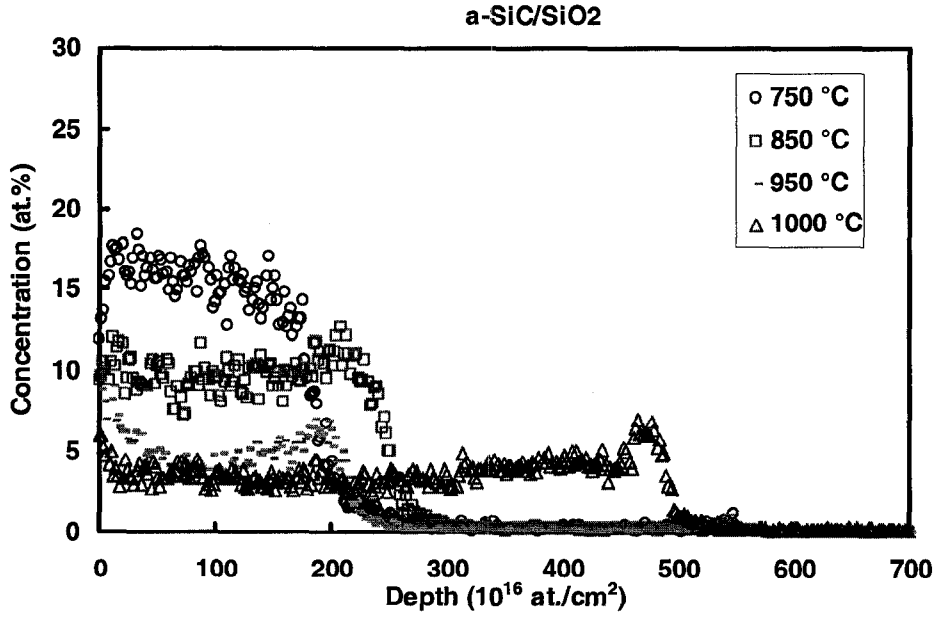

Figure 5-4 Oxygen concentration in the films deposited at temperatures of 750, 850, 950 and 1000 °C on SiO_2 substrate

The CV characterization of the films is presented in figures 5-5 to 5-8 for different deposition temperatures. These results show semiconductor characteristics for the films deposited at 1000 °C. Most of the a-SiC thin films deposited at this temperature under non-intentional doping conditions show intrinsic n-type behaviour. By decreasing the deposition temperature, the deposited films exhibit increasingly insulating behaviour, while the capacitance remains constant. The CV curves for the samples deposited at temperatures between 750 °C to 950 °C on n-type silicon are shown in figure 5-5. The CV curves of these samples have a constant value when the material remains in forward bias (positive voltage). This constant value corresponds to the capacitance of deposited a-SiC and indicates an insulating behaviour for these films. Above 950 °C, the a-SiC thin film starts to conduct, so the capacitance in the maximum part of CV curves is no longer constant, because of depletion in a-SiC layer deposited on silicon substrates.

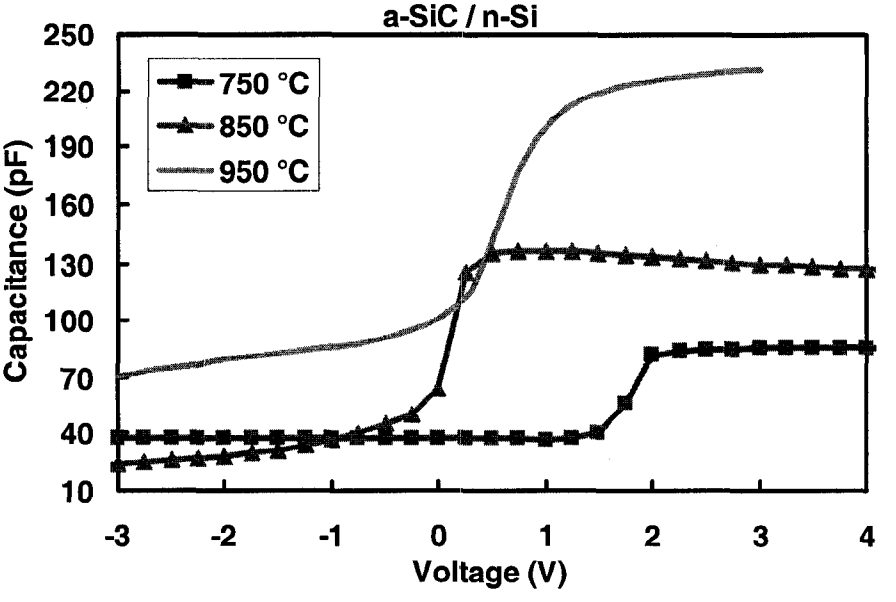

Figure 5-5 CV curve of thin film deposited at 750 °C, 850 °C, and 950 °C on n-type silicon substrate

The similar behaviour is observed for the films deposited on p-type silicon at similar temperatures (figure 5-6). The transient part of the CV curves for the samples deposited at lower temperatures corresponds to the depletion in the silicon substrate. The minimum part of the CV curves shows the saturation of charges in the silicon substrate, and the flat shoulder at this part may be caused by the inversion of charges affected by the interface of a-SiC/p-Si. Again, the semiconductor properties of the material that appear above 950 °C, related to the observed transient capacitance at the maximum part of CV curves.

Since the films are very thin, the breakdown happens right after conduction in the n-type deposited a-SiC thin film. Figure 5-7 shows the CV curves of the samples deposited on silicon dioxide substrates over the same range of temperature. Lower than 950 °C, the a-SiC films are clearly insulating. However, above 950 °C all samples show semiconducting behaviour. When increasing the temperature to 1000 °C, the films deposited on all substrates have n-type semiconducting behaviour.

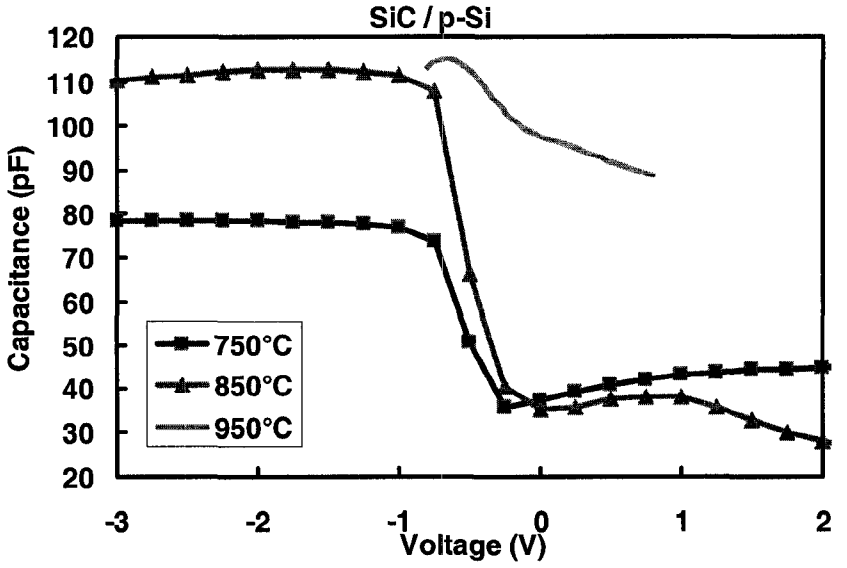

Figure 5-6 CV curve of thin film deposited at 750 °C, 850 °C, and 950 °C on p-type silicon substrate

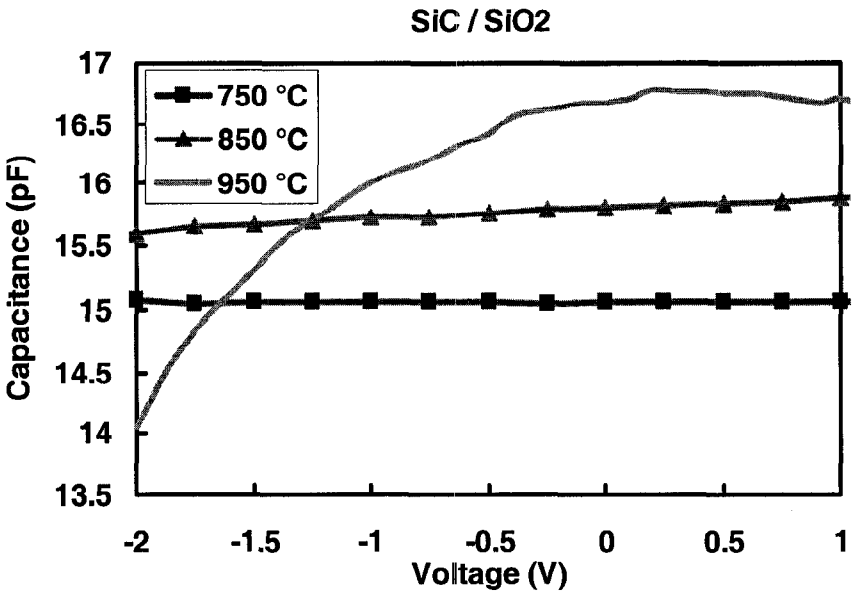

Figure 5-7 CV curve of thin film deposited at 750 °C, 850 °C, and 950 °C on silicon dioxide substrate

Figure 5-8 shows the CV curves of the material deposited at 1000 °C; (a) on n-type, (b) on p-type, and (c) on SiO_2 substrate. As presented in figure 5-8(a) the change of capacitance for the sample deposited on n-type silicon is observed to be about 10 pF between -1 to 1 V. The CV results for the films deposited on p-type substrate at 1000 °C are shown in figure 5-8(b). This CV curve indicates an n-type material when the measured capacitance increases about 10 pF between -1 to 1 V. Deposition on SiO_2 also indicates semiconductor behaviour, as shown in figure 5-8(c). This film is also an n-type material for which the capacitance change is 7 pF between -1 to 1 V.

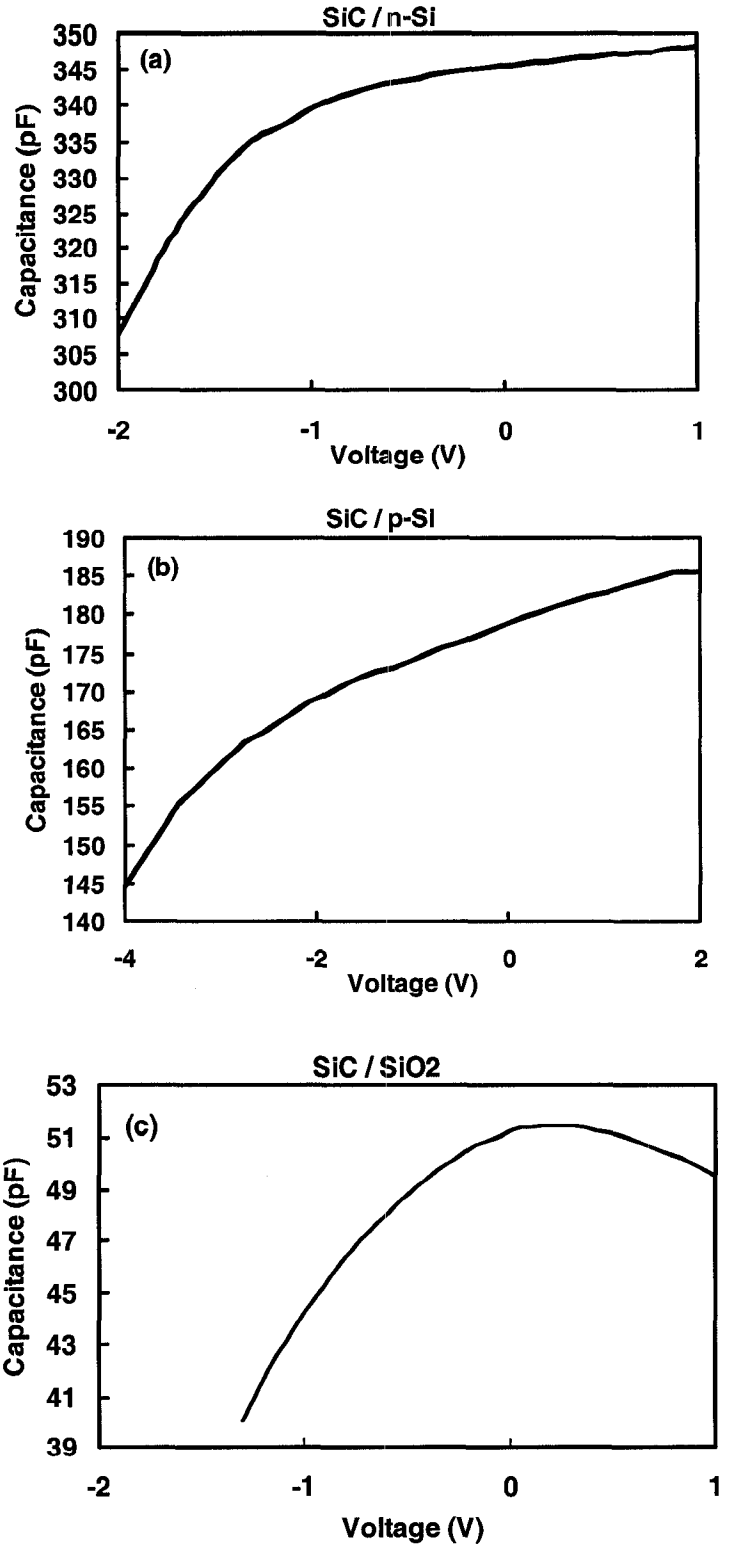

Figure 5-8 CV curve of thin film deposited at 1000 °C, (a) on n-type silicon, (b) on p-type silicon, (c) on silicon dioxide

5.2. Contact characterization

The electrical properties of Ni contacts deposited on a-SiC surface have been tested by IV measurements. The characteristics of the contacts depend on the properties of the deposited film and on the subsequent rapid thermal annealing process. IV curves for the nickel contacts deposited on semiconducting sample prepared at 1000 °C and on SiO_2 substrate are shown in figure 5-9. The Schottky behaviour for the contacts was observed before annealing, which is presented in figure 5-9(a). After annealing at 800 °C for 2 min, the behaviour was changed to ohmic one, which is indicated in figure 5-9(b). The appearance of the ohmic behaviour after annealing can be caused by the interaction of a-SiC with the Ni contact at the annealing temperature, which leads to a change of the a-SiC properties near the interface. The formation of the graphite phase at the surface was reported at high temperature annealing [Nikitina et al., 2005], which indicates that the C atoms diffused out to the surface at high temperature. This leads to the formation of carbon vacancies, acting as donors. It can be concluded that the production of carbon vacancies plays a major role in the formation of ohmic contact through the reduction of the effective Schottky barrier height for the transport of electrons, which has been also indicated by Han et al. [Han et al., 2002].

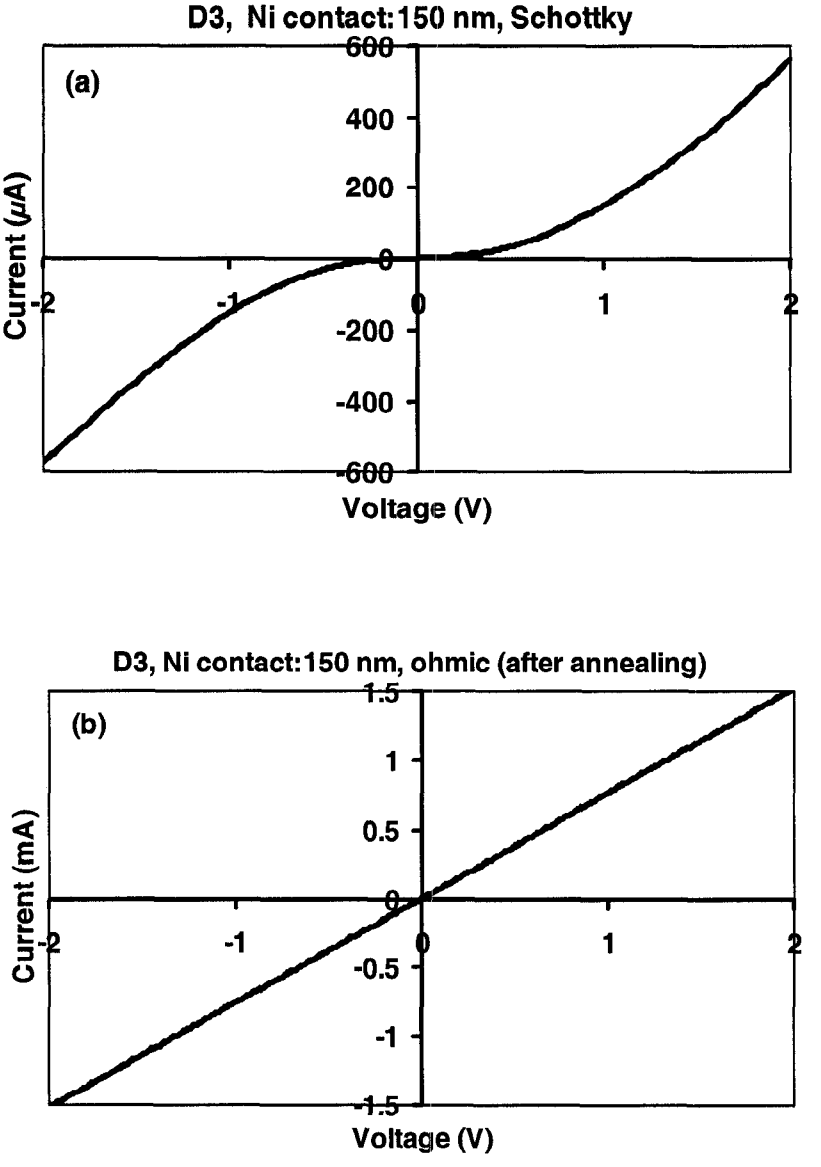

Figure 5-9 Current-voltage characteristic of nickel contact of deposited thin film at 1000 °C (a) before annealing, (b) after annealing

5.3. Results of mobility measurements

Due to the high resistivity of the a-SiC samples which have been prepared at temperatures lower than 1000 °C, some difficulty was encountered in the Hall Effect measurements of these samples. As it was explained in section 4.2.1, a DC current should be adjusted on the current source to be applied to the sample, which is object for the Hall measurements. Conditionally, the power dissipation should not exceed 5 mW (preferably 1 mW). This limit has been set as $I< (200R)^{-0.5}$, which R was the resistance between any two opposing leads (1 to 3 or 2 to 4). Thus, the currents which were adjusted for the high resistive samples were too low and could not be affected significantly in the Hall Effect measurements. These samples, which had been deposited at low temperatures, were considered as the low mobility samples.

As explained in section 5.1, by increasing the deposition temperature the conductivity of the films augment. The elemental composition of such a film as resulted from ERD has been presented in Figure 5-10. Increased carbon concentration has been observed by comparing these results with the ERD results on a-SiC films deposited at lower temperatures, as shown in figure 5-2(c). This higher value of the carbon concentration could affect the conductivity of the material, by adding more impurity levels in its band gap resulting in an increase of the mobility of material.

The mobility measurements were successfully done for the samples deposited on SiO_2 substrate at 1000 °C. The average mobility of three similar samples gives the value of μ_H = 34 $cm^2/V.s$, which was obtained using the calculating procedure explained in chapter 4.2.1.

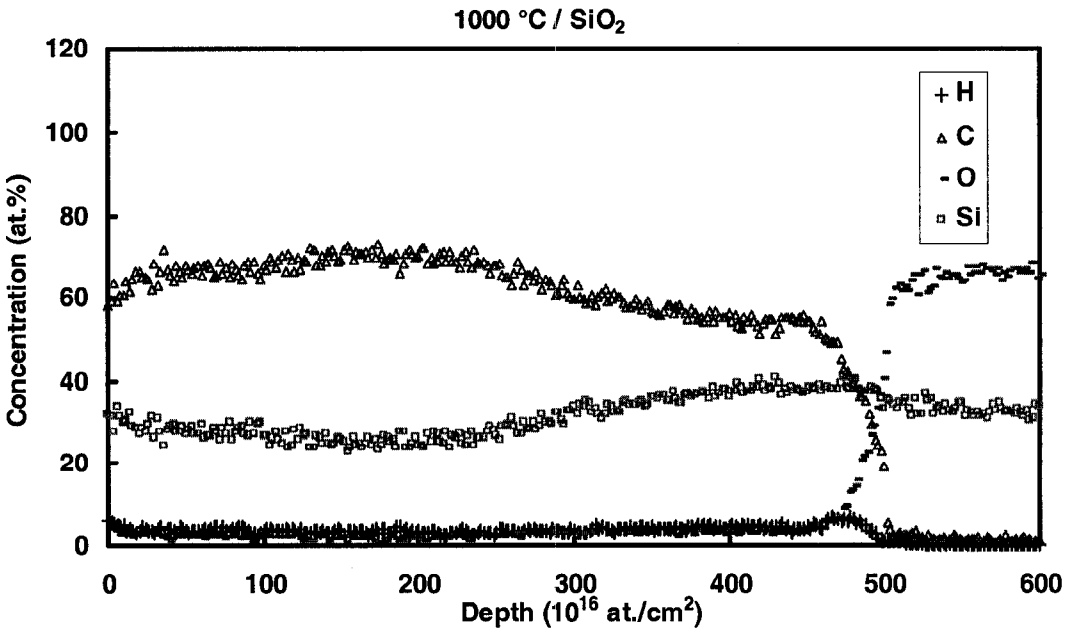

Figure 5-10 ERD measurement of the thin film deposited at 1000 °C on SiO_2 substrate

CHAPTER 6: APPLICATION OF A-SIC LAYERS IN CONTACT BARRIER DIODES

The a-SiC thin films are widely used in semiconductor devices. The material itself has a wide band gap, varying from 1.5 to 4 eV depending on the deposition conditions. This may lead to potential applications based on the optical and electrical properties of this material [Jung et al., 2002]. Recently, nano-size thin films have been used for the modification of semiconductor Schottky contacts in order to improve the device performance by adjusting its barrier height [Bolognesi et al., 2003]. Other proposed mechanism to tune the barrier height employs hydrogen which introduces a positive charge on the semiconductor side of the interface. The utilization of monolayers of small molecules whose dipole moment is varied systematically is another proposed mechanism for tuning the effective barrier height [Vilan et al., 2000].

In this work, a-SiC is used as an interlayer for the modification of Ni/p-Si(100) Schottky contacts. The a-SiC films were deposited by polymeric source chemical vapour deposition (PS-CVD) technique at atmospheric pressure. The deposition temperature was 750 °C and the substrate was p-type silicon (100) with resistivity in the range of 1-10 Ω.cm. Three samples of a-SiC were prepared by single-step deposition. The optical band gap of the deposited a-SiC was determined to be about 3.6 eV from UV-VIS absorption data. Aluminium was evaporated at broad back side of silicon, and nickel circles with area of 7.85×10^{-3} cm^2 were evaporated onto the surface of a-SiC to form the ohmic contacts. The thicknesses of the films directly under Ni contacts were determined by the ERD method, which was already explained in section 4.2.2. Typical composite depth profile plots from ERD experiments are shown in Figure 6-1. The results of the first sample containing ~215 nm of an a-SiC interlayer are shown in 6-1(a). The two other samples of ~270 nm show nearly similar film thicknesses for the a-SiC layers, as shown in 6-1(b) and (c). The a-SiC film compositions underneath the Ni contact as well as very near region outside Ni circle were nearly identical with experimental errors for all the samples. However, these samples may be different in the case of trap density, because they will be resulted in different IV and CV characteristics. The electronic transport properties of Ni/a-SiC/p-Si contact barrier diodes

are investigated using IV and CV measurements. IV measurements were done using HP4145A semiconductor parameter analyser. A 1260 Schlumberger instrument was used for the CV measurements. The results are presented in sections 6.1 and 6.2. By considering the thermionic emission-space-charge-limited current model, the IV results were used to calculate the characteristics of a-SiC thin film. The calculation methods and the obtained results are discussed in section 6.3.

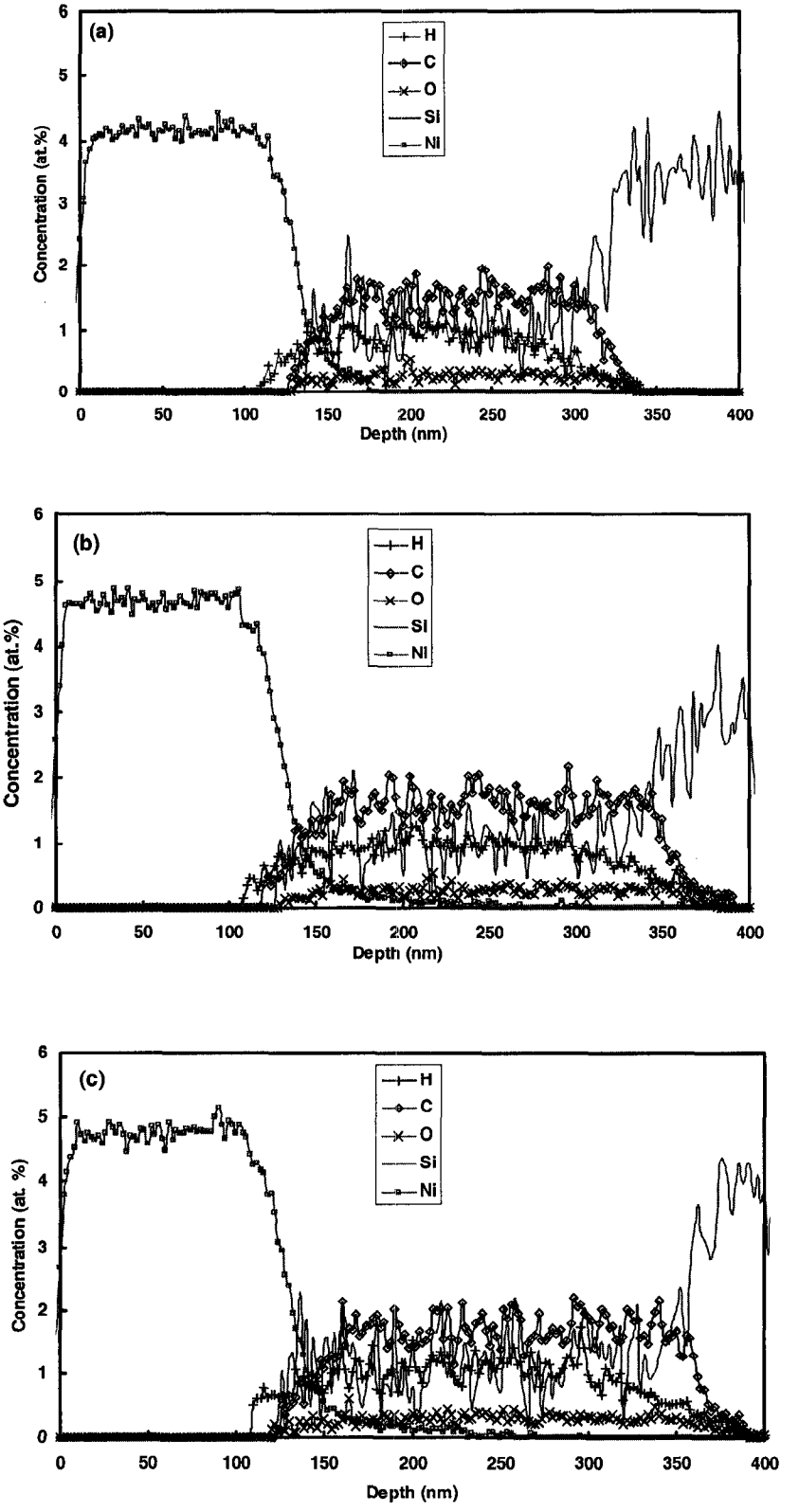

Figure 6-1 ERD depth profiles of elements in Ni/a-SiC/p-Si/Al diodes for the thickness of a-SiC layer; a) 215 nm, b) 270 nm, and c) 270 nm.

6.1. IV characteristics

Figure 6-2 shows the IV characteristics of the Ni/a-SiC/p-Si/Al devices at the room temperature, where the a-SiC thicknesses were 215 nm in one sample, and 270 nm for two others. As explained earlier, a-SiC is intrinsically an n-type material. However, most of the incorporated impurity atoms in a-SiC are in an electronically inactive state and the equilibrium carrier densities n_0 is small in this material. Reversible changes of this doping efficiency give rise to a change in the density of shallow majority carriers, which is observable through conductivity measurements. In the Ni/a-SiC/p-Si structure, holes are injected from the p-contacts into the intrinsic a-SiC layer. Then, the current through this biased diode is, almost exclusively due to the majority carriers injected into the intrinsic region. For a sufficiently large current through the diode, many excess carriers are injected and the quasi-Fermi level of the majority carriers can be shifted towards the valence band. In the IV characteristics of figure 6-2, this shift can be observed as a deviation from the ohmic behaviour toward a strongly superlinear current-voltage characteristic (SCLC). The difference between samples (a) and (b) could be related to the density of midgap defects. A sample with a large density of midgap defects will show a lower overall conductance and will require higher fields for a deviation from ohmic behaviour than it is required in the low-defect density samples [Kanicki, 1991]. Sample (a) shows a lower current and a higher barrier height compared to sample (b) with the same thickness of a-SiC. This led to the conclusion that the high trap density causes the higher resistivity material. As shown in figure 6-2, the measured forward currents have two distinct regions. In the low forward voltage region (V < 0.5 V), the behaviour can be described by an exponential function which can be written as:

$$-I = I_s\left[\exp\left(\frac{-qV}{nkT}\right)-1\right] \qquad (6\text{-}1)$$

where I_s is the saturation current, k is the Boltzmann's constant, T is the absolute temperature, q is the electron charge, and n is the ideality factor.

The ideality factors, obtained from the slop of the linear part in exponential regions of the curves (figure 6-3), and the saturation currents are summarized in table 6-1. The values of n may correspond to the carrier recombination in the amorphous side due to the trap distribution with a high density of tail states. The value of n ranges from 1.15 to 2.5, and are not in order of the a-SiC thicknesses. The saturation current across the contact barrier is given by:

$$I_s = -A^* T^2 \exp\left[-q(\phi_{Bp})/kT\right] \qquad (6\text{-}2)$$

Here, A* is the effective Richardson constant and equals to 32 A/cm^2 K^2 for p-type Si and ϕ_{Bp} is the barrier height.

The apparent barrier heights obtained for the three samples are added also to the table 6-1. There is no pronounced dependence of ϕ_{Bp} on a-SiC thickness is a characteristic of the a-SiC/p-Si contact which influences the value of saturation current. Comparing the calculated barrier height of the sample (a) having a thickness of 270 nm a-SiC, with the calculated barrier height of the first sample having a thickness of 180 nm a-SiC, indicated that these two samples made nearly the same barrier with c-Si. It could be concluded that the density of states in a-SiC for these two samples are similar. However, the ideality factor depends on the resistivity of the interlayer, therefore is changed with thickness of amorphous interlayer as well as the density of states. From table 6-1, it is observed that the sample (a) has the highest ideality factor, $n=2.5$, as compared to the other samples. The value of $n=1.15$ for sample (b) suggests that the apparent barrier height, which will be obtained from analyzing the forward IV data, is close to the ideal barrier height.

At higher forward currents, the IV characteristics are useful for studying SCLCs in the contact barrier devices. Figure 6-4 shows the forward current characteristic on a log-log scale. As it can be observed, for $V>0.5$ V, the current increase superlinearly which is the characteristic of SCLC. In this region, the effective resistance of the a-SiC will control the diode current. Under these conditions the current-voltage relationship is given by: $I = kV^m$

with $m>1$. The dominant conduction mechanism is SCLC when sufficient carriers are injected into the a-SiC layer so that the resulting space charge from the injecting contact extends across the entire sample width. The current flow may then significantly exceed the ohmic current. The actual relationship between the current and voltage is depend on the distribution of traps in the a-SiC and the thickness of this amorphous layer. The values of k and m obtained by fitting in high voltage region ($V>0.5$) of IV curves shown in figure 6-4. These are given in Table 6-1. This relationship between current and voltage is consistent with equation (3-12) for SCL currents. k has the lowest value for the device with a low forward current due to the high defect density in a-SiC. The value of m depends on the thickness of the a-SiC layer and has the highest value for the lowest thickness.

TABLE 6-1 ELECTRICAL PROPERTIES OF NI/A-SIC/P-SI CONTACT BARRIER DIODES OBTAINED FROM IV ANALYSIS

Sample thickness	I_0 (A/cm^2)	n	Φ_{Bp} (eV)	m	K
215 nm	1×10^{-7}	1.5	0.77	2	1.2×10^{-3} (V^{-2}.A/cm^2)
270 nm-a	8×10^{-8}	2.5	0.78	1.65	1×10^{-5} ($V^{-1.6}$.A/cm^2)
270 nm-b	2×10^{-6}	1.15	0.7	1.7	3.3×10^{-3} ($V^{-1.7}$.A/cm^2)

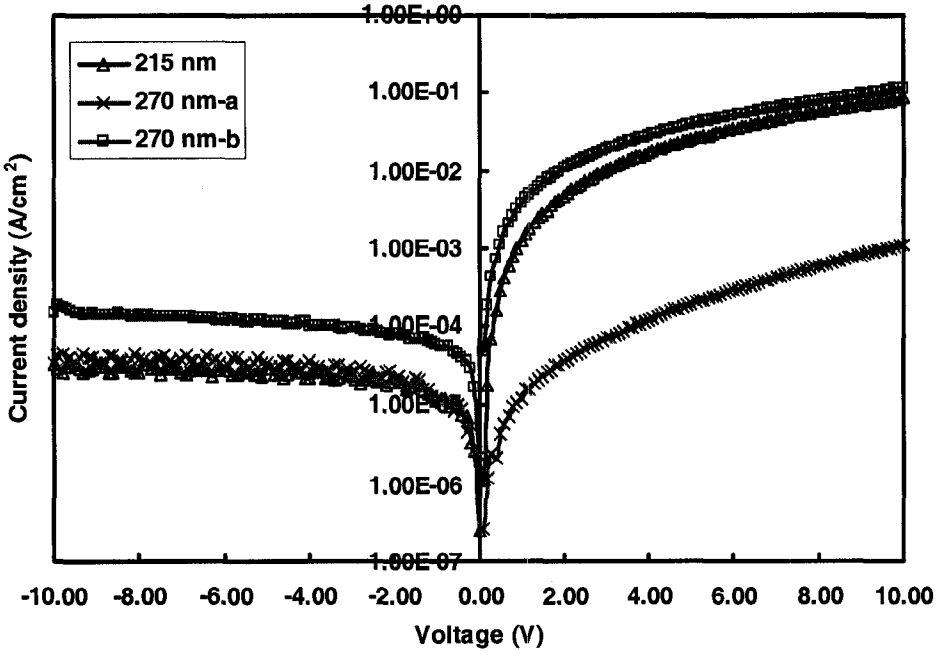

Figure 6-2 IV curves of the Ni/a-SiC/p-Si heterostructures

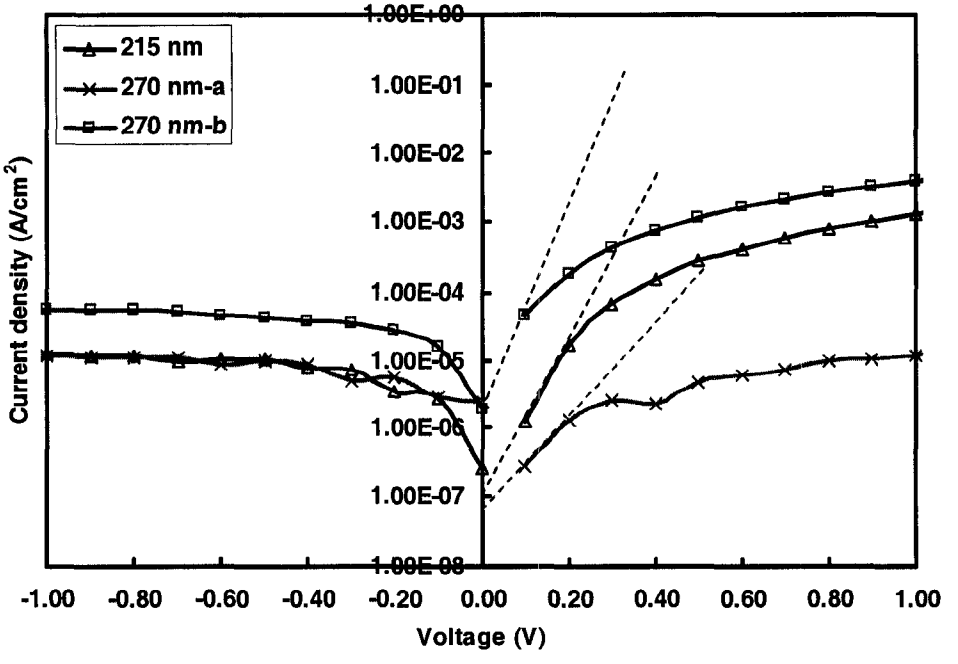

Figure 6-3 Low voltage region of the IV curves used for saturation currents and ideality factors calculation

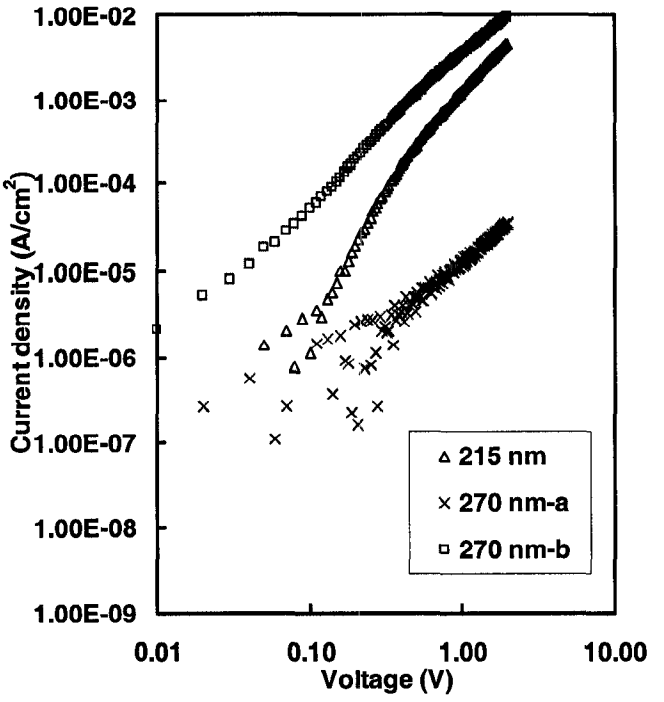

Figure 6-4 Forward current characteristic on a log-log scale of the Ni/a-SiC/p-Si devices

6.2. CV characteristics

Figure 6-5 shows the high-frequency CV characteristics of the Ni/a-SiC/p-Si heterostructures. The CV curve of sample (a) with 270 nm a-SiC exhibits a broadening along the voltage axis. This is due to the additional contribution from the interface states to the surface states of silicon. Thus, a larger gate bias is required to produce the same degree of band bending in silicon compared to sample (b) which has the same thickness of a-SiC. On the other hand, the CV curve of sample (a) shows a higher capacitance compared to sample (b). This can be attributed to the a-SiC gap states contribution. The reason is that the density of charged gap states is equal and of opposite polarity to the total space charge in Si that determines the capacitance in positive voltages. Therefore, the sample (a) which shows higher capacitance has higher density of gap states.

As it is seen in figure 6-5, the measured capacitance of a-SiC layer (negative voltages) shows a weak dependence on the applied voltages and the measured frequency of 1 MHz is three

orders of magnitude higher than the cutoff frequency (ω_c). Therefore the undoped films can be treated as dielectric. This assumption is correct because the typical conductivity (σ) of undoped a-SiC is 1×10^{-9} $(\Omega\ cm)^{-1}$ at the room temperature, its dielectric constant (ε_a) is approximately 4-10 then, ω_c, which is equal to $\sigma/\varepsilon\varepsilon_0$, will be in the kHz range [CHEW et al., 2001]. Adopting this assumption, the a-SiC film capacitance, C_a, is determined from the strong accumulation region of the CV curves by relation of $C_a= \varepsilon_a\varepsilon_0 A/d$, where A is the area of the Ni contact, and d is the thickness of a-SiC film. Using this relation, the values of ε_a were obtained for the three samples are presented in table 6-2. As it is shown in figure 6-5, C_a is not proportional to $1/d$ over the range of thickness used, suggesting that pinholes and other film defects are high in number and have large effect on device behaviour. The monolithically increasing of diode capacitance with voltage in forward bias can be explained by the parallel combination of the space-charge resistance $R_{sc}(V_{sc})$ and capacitance C_a which makes it different from MIS devices.

The curves of A^2/C^2 versus V are plotted in figure 6-6. The linear trend of the plots of A^2/C^2 versus bias voltage is clear from this figure indicating that the a-SiC/p-Si heterojunction is abrupt. The slope of the plot is inversely proportional to the net carrier concentration (N_A) in the Si substrate. The values of the net carrier concentration in Si, were calculated by a procedure similar to that used for the Schottky barrier diodes, and the results are shown in table 6-2. The value of the built in potential, V_{bi}, was obtained from the intercept of the straight lines with the voltage axis. These values are presented in table 6-2. Using the values of V_{bi} and N_A, the barrier heights for the holes (Φ_{Bp}) were calculated, and the results are presented also in table 6-2. These barrier heights are much different than the values obtained from IV characteristics. However, the A^2/C^2 versus V characteristics are nonlinear near V=0 due to the presence of the fixed positive charge in the interface region. This may be partially responsible for the large barrier height (Φ_{Bp}). The nonlinear behaviour near V=0, makes it hard to accurately determine Φ_{Bp} from V_{bi} by CV analysis.

TABLE 6-2 ELECTRICAL PROPERTIES OF NI/A-SIC/P-SI CONTACT BARRIER DIODES OBTAINED FROM CV ANALYSIS

Sample thickness	Dielectric constant (ε_a)	V_{bi} (V)	Φ_{Bp}(eV)	N_A (cm^{-3})	W_0 (nm)	n_0 (cm^{-3})
215 nm	3.28	0.5	0.74	2.03×10^{15}	5.8×10^{-5}	3.93×10^{15}
270 nm-a	4.2	0.15	0.4	2.78×10^{15}	2.8×10^{-5}	2.66×10^{15}
270 nm-b	3.76	0.9	1.14	1.73×10^{15}	8.3×10^{-5}	5.57×10^{15}

As discussed in chapter 3, due to the low carrier density at equilibrium (n_0) in the a-SiC layer, the carrier injection from Si charges the entire a-SiC film and raises the Fermi level close to the valence band edge. As a result, the material becomes p-type. The p-type characteristics can be seen in figure 6-5 for two of the samples. Sample (b) does not show the p-type characteristics which may result from the large thickness of the a-SiC layer and the lower trap density in this material. It can be concluded that the carrier density at equilibrium n_0, in sample (b) is higher than the carrier density at equilibrium in sample (a), even though both have same thickness. Therefore, the maximum thickness (d_{max}) at which an a-SiC film which becomes p type by charge injection is different for each sample. However, if the value of n_0 could be determined for each sample, the quantity d_{max}, which is the distance from the a-SiC/p-Si interface over which band bending in a-SiC extends, could be obtained by the procedure presented below.

The amount of charge per unit area in the interfacial dipole barrier layer is roughly $N_A W_0$, where W_0 is the equilibrium depletion region width, obtained from the following equation:

$$W = \left(\frac{2\varepsilon_{Si}\varepsilon_0 (V_{bi} + kT/q)}{qN_A} \right)^{1/2} \tag{6-3}$$

Since $n_0 d$ is the total free electron concentration in the uncontacted material, d_{max} could be approximately calculated using the equation below:

$$n_0 d_{max} = N_A W_0 \tag{6-4}$$

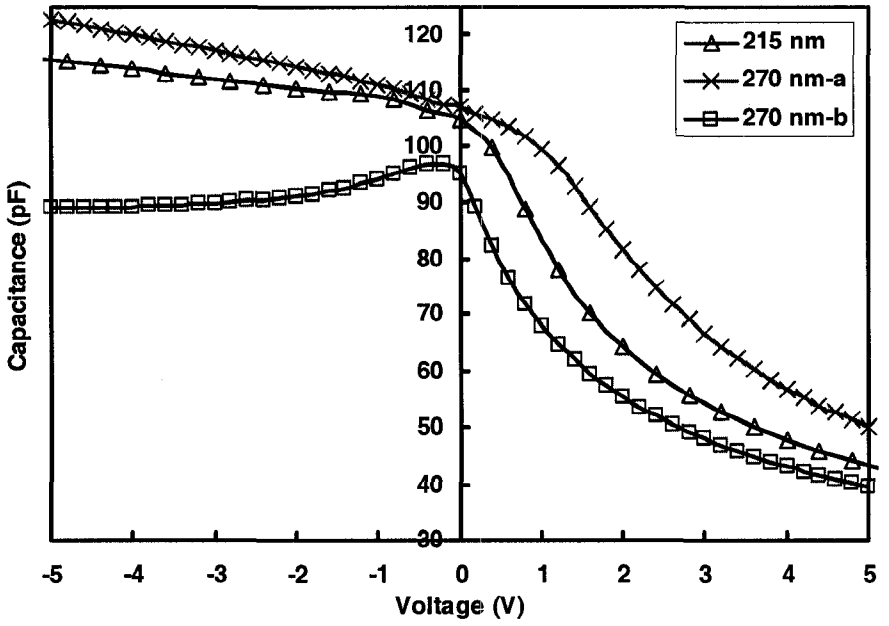

Figure 6-5 CV curves of the Ni/a-SiC/p-Si heterostructures

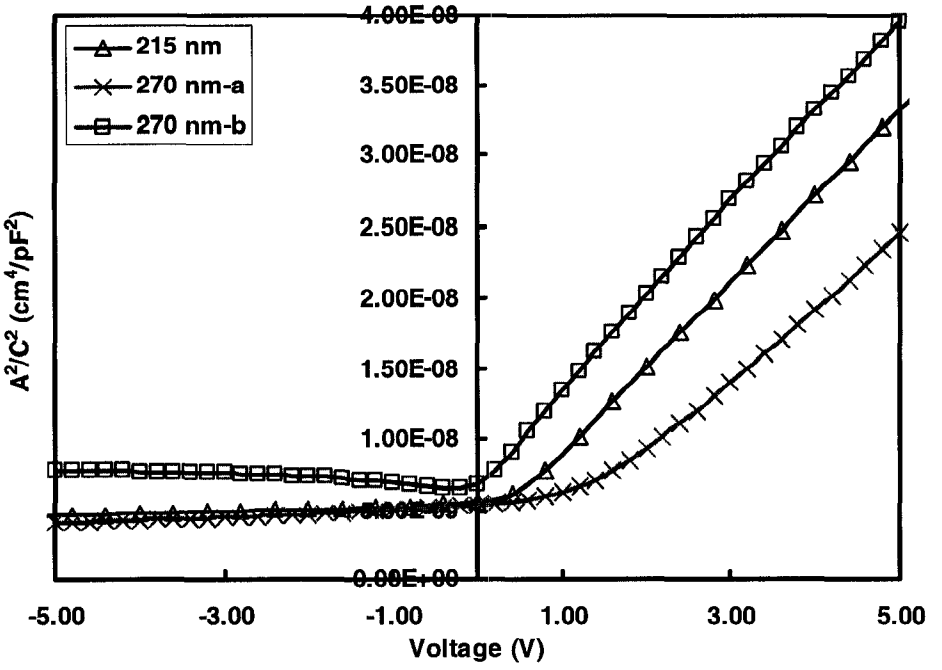

Figure 6-6 A^2/C^2 vs. voltage for the Ni/a-SiC/p-Si heterostructures

6.3. Mobility and lifetime calculation

The heterojunctions between the amorphous material and the crystalline silicon can be used to obtain some of the properties of the amorphous layer. In this section, the IV characteristic of the Ni/a-SiC/p-Si devices is used to calculate the properties of the a-SiC layer, such as mobility and carrier lifetime. It was indicated before that the direct measurement of such properties in a-SiC is difficult, due to the high resistivity of this material. Here, the backward theory of SCLC in Ni/a-SiC/p-Si devices, which was explained in chapter 3, is used for the calculation of such properties. The calculation procedures will be explained in this section.

The dependence of the total space charge limited current (J) on the voltage drop across the space charge region (V_{sc}) was estimated by Mont-Gurney relation:

$$J = \frac{9}{8}\varepsilon_0\varepsilon_a\mu_{eff}\frac{V_{sc}^2}{d^3} \qquad (6\text{-}5)$$

where μ_{eff} is the apparent mobility of a-SiC and contains the effect of trap density in a-SiC. Across the a-SiC/p-Si contact barrier, the current is due to thermionic emission, and can be expressed as follow:

$$-J = J_s[\exp(-qV_D / nkT) - 1] \tag{6-6}$$

where V_D is the voltage drop across the p-Si semiconductor, and J_s is the saturation current. The measured current was used to calculate V_D using equation 6-6, by applying the value of n, which is indicated in table 2.

The total voltage drop across the device series resistances (R) is given by

$$V_R = (RA)J \tag{6-7}$$

where A is the contact area. From the literature [Han et al., 2002], the resistance of the ohmic contacts obtained on SiC using Ni was reported to be lower than $RA=3.3\times10^{-3}\ \Omega.cm^2$. This value was used here for the calculation of V_R, using equation 6-7.

An equivalent circuit was considered for the contact barrier diode, which is shown in figure 6-7.

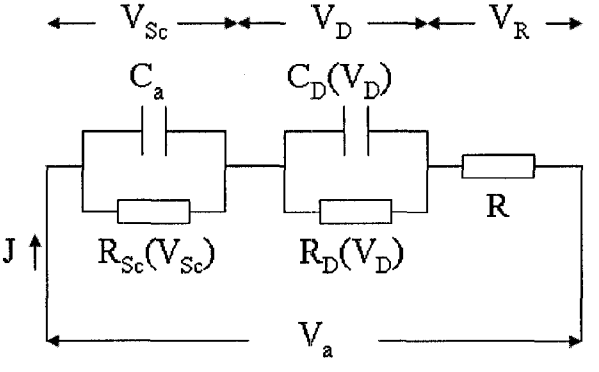

Figure 6-7 Equivalent circuit of contact barrier diode

Considering this circuit, the applied voltage could be assumed as the sum of the three voltages: the voltage drop across the a-SiC layer (V_{Sc}), the voltage drop across the p-Si substrate (V_D), and the voltage drop across the series resistance (V_R).

V_{sc} will be obtained from following equation where V_D and V_R have been already calculated from equations (6-6) and (6-7):

$$V_{sc} = V_a - (V_D + V_R) \tag{6-8}$$

By substituting the obtained values of V_{sc} in equation (6-5), the experimental values of the effective mobility of a-SiC, μ_{eff}, for the three samples were calculated. The plots of mobility versus applied voltages are shown in figures 6-8 and 6-9. The values of μ_{eff}, when the space-charge effects limit the forward current characteristics of the device ($V_a > 0.5$ V), are lower than the actual mobility, due to the high electric field across the a-SiC. The effective mobility is nearly constant at higher voltage, and ranges from 10^{-7} to 10^{-4} cm^2/Vs. The variation in the mobility over several orders of magnitude for different samples is probably due to the variations in the ratio of trapped carriers to free carriers induced by various defect densities in each a-SiC sample. The effective mobility is indicative for the role of traps in the charge transport in a-SiC. The rapid decrease of the calculated effective mobility at lower forward voltages is due to the exponential dependence of V_{sc} on V_a, which is shown in figure 6-10. The decreasing of μ_{eff} continues until the space-charge effects limit the forward current characteristics of the device.

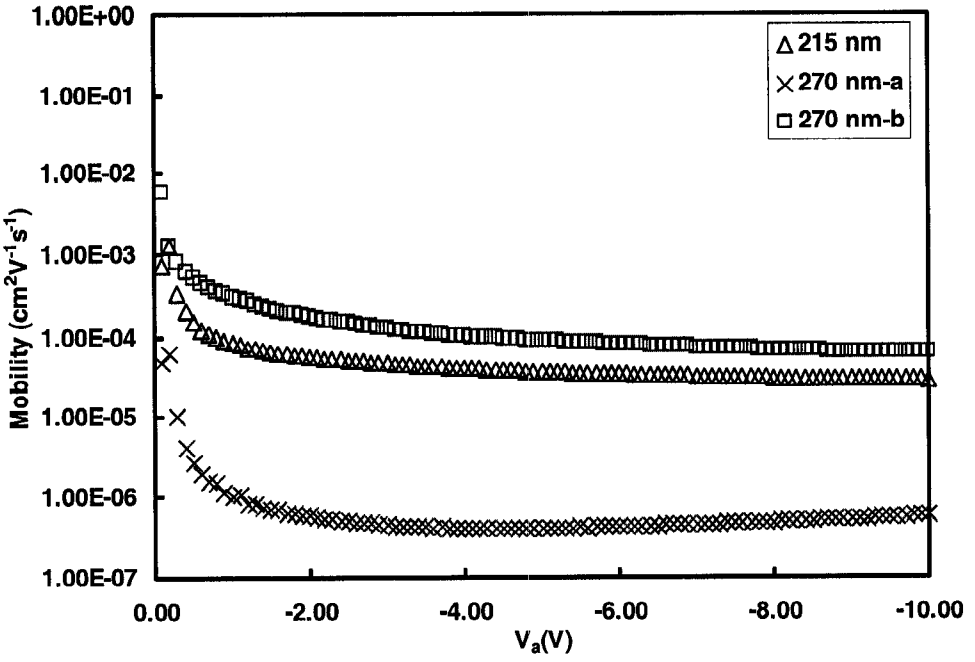

Figure 6-8 Effective mobility of a-SiC (μ_{eff}) vs. applied voltage (V_a) for higher forward biased Ni/a-SiC/p-Si contact barrier diodes

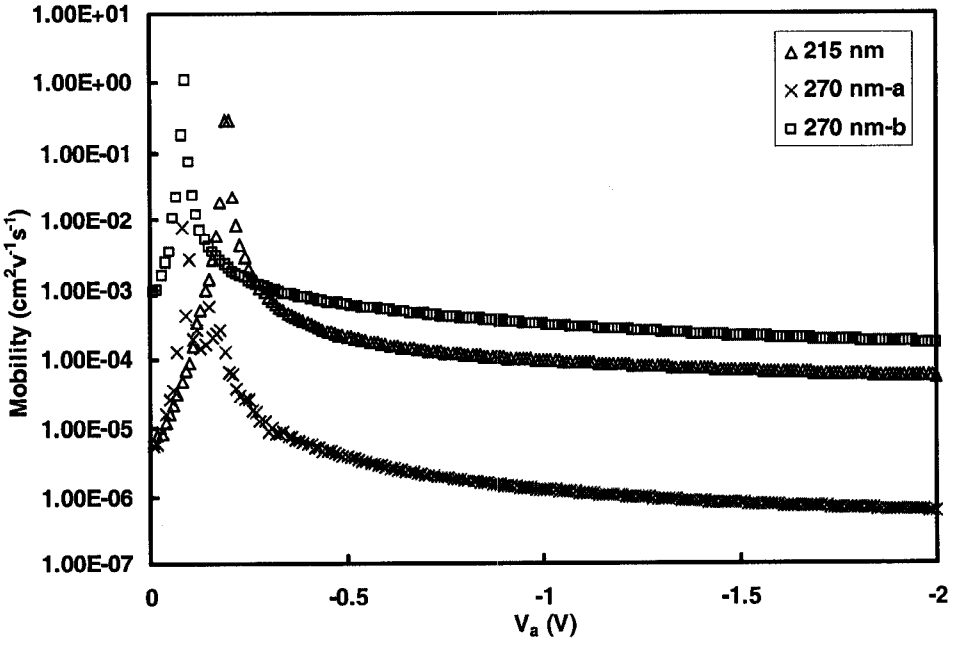

Figure 6-9 Effective mobility of a-SiC (μ_{eff}) vs. applied voltage (V_a) for lower forward biased Ni/a-SiC/p-Si contact barrier diodes

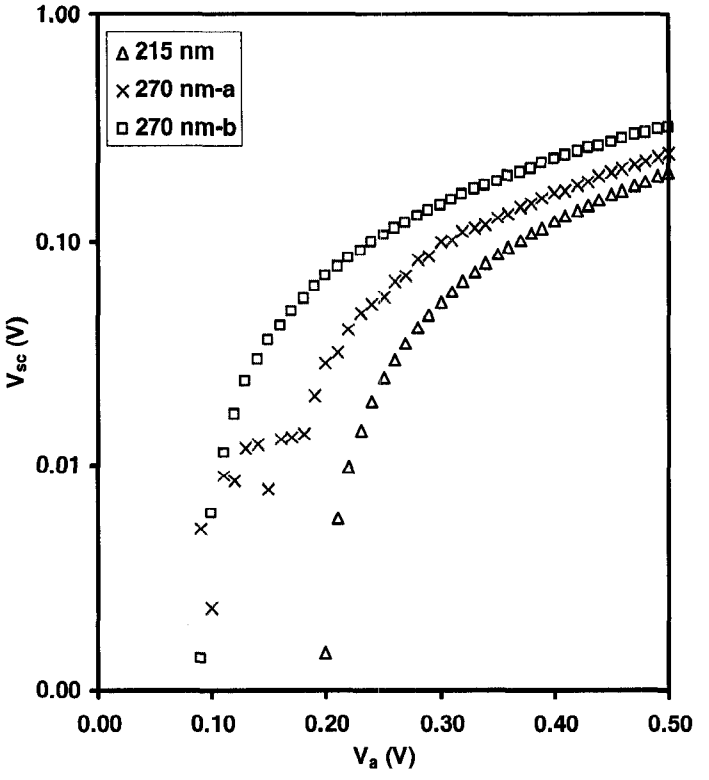

Figure 6-10 Voltage drop across the organic layer (V_{sc}) vs. applied voltage (V_a) for Ni/a-SiC/p-Si devices

The transit time of carriers across the space-charge layer can be estimated by $\tau = d/v$ where v is the velocity of carriers and is given by $v = \mu_{eff} E_{sc}$. The electric field in the space-charge layer, E_{sc}, can be obtained from equation 3-18. Therefore, the carrier lifetime across the a-SiC layer can be estimated by the following equation:

$$\tau \approx \frac{d^2}{\mu_{eff} V_{sc}} \tag{6-8}$$

This indicates that τ decreases with increasing V_{sc}. In figures 6-11 and 6-12, the calculated transit time is plotted versus the applied voltage for the contact barrier devices. At lower forward voltage, the carrier lifetime is small and increases rapidly due to the exponential

dependence of V_{sc} on V_a (figure 6-12). It can be concluded that the switching time of the thin film device is not limited by the relatively low mobility of a-SiC layer.

The electric fields in the crystalline substrate and in the amorphous interlayer, versus current density, are plotted in figure 6-13 for the device with 215 nm a-SiC. The fields were calculated using equations 3-17 and 3-18, respectively. It can be concluded that the highest electric fields are developed in the silicon substrate at low current densities, and at high currents, the highest fields are in the amorphous thin film, as is expected for thermionic emission-space-charge-limited current. This result confirms that the IV characteristic of the contact barrier diodes, at higher current, can be used to determine the characteristics of the amorphous thin film interlayer.

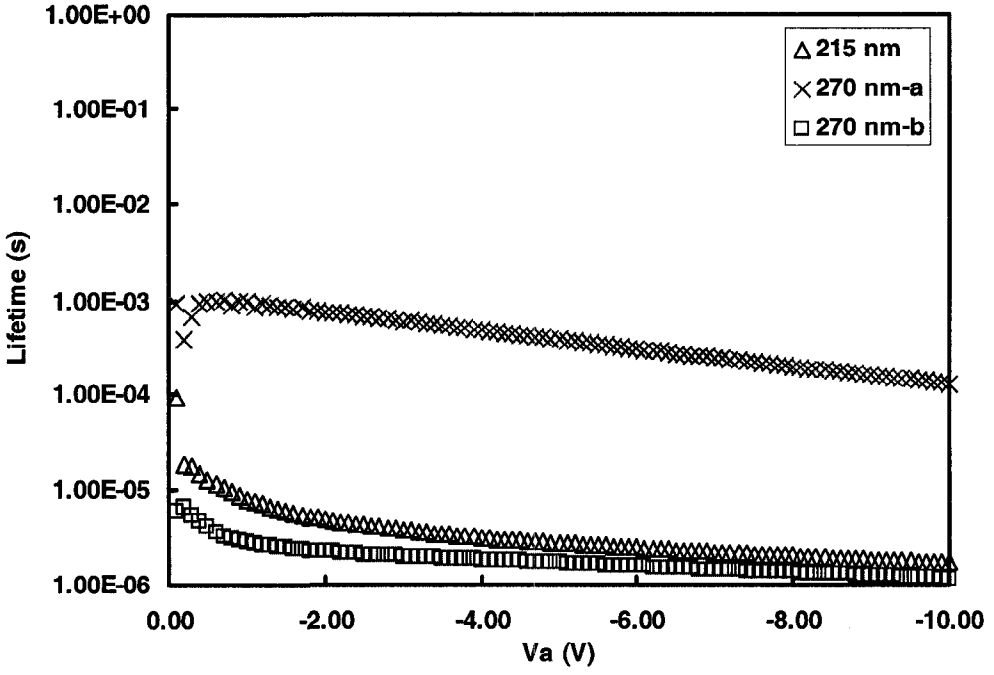

Figure 6-11 Lifetime of injected carriers (τ) vs. applied voltage (V_a) for higher forward biased Ni/a-SiC/p-Si contact barrier diodes

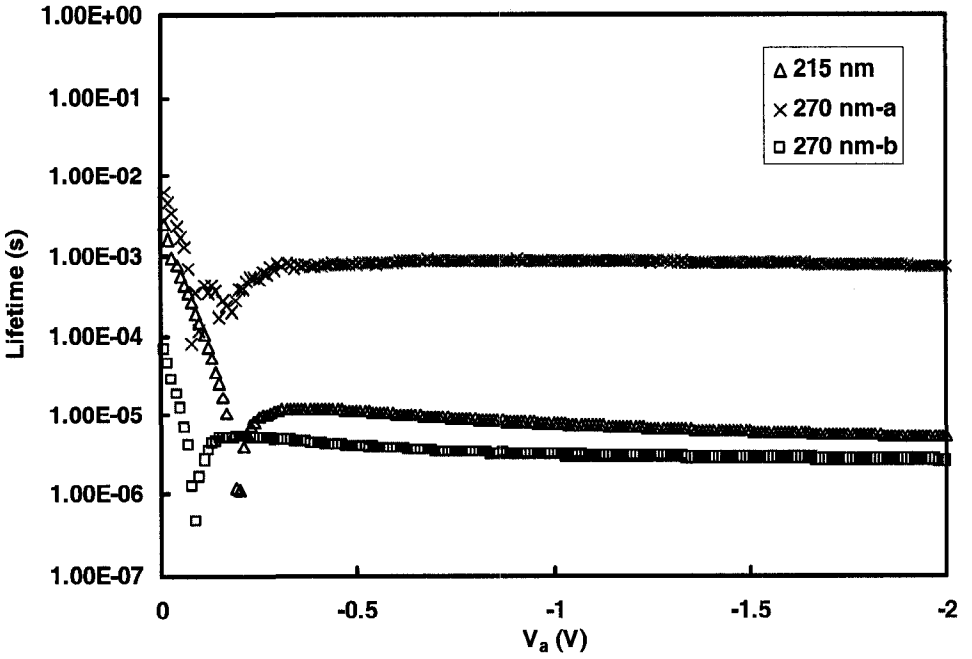

Figure 6-12 Lifetime of injected carriers (τ) vs. applied voltage (V_a) for lower forward biased Ni/a-SiC/p-Si contact barrier diodes

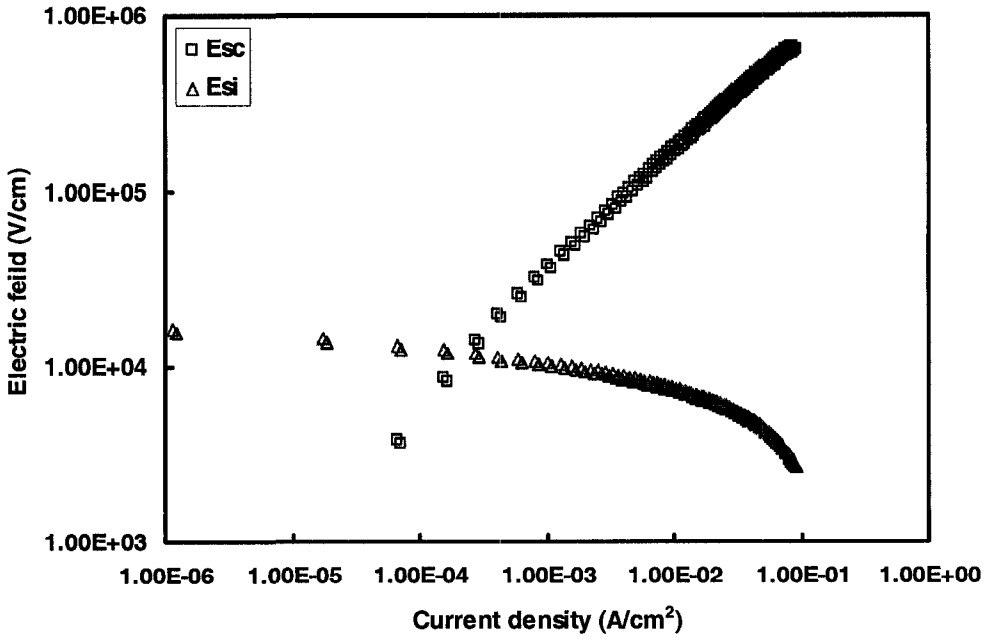

Figure 6-13 Electric field in the space-charge layer (E_{sc}) and in the substrate (E_{si}) of Ni/a-SiC/p-Si contact barrier diode

CONCLUSION

A comprehensive study on the chemical and electrical properties of intrinsic a-SiC thin films and on the applications of this material in the contact barrier devices were presented. At this work, for the first time, it was done:

- Deposition of a-SiC thin film using polymeric solid source.
- A comparison between chemical and electrical characterization methods to study the conductivity of a-SiC in a range of deposition temperatures from 750 ^{o}C to 1000 ^{o}C.
- Mobility measurements of high temperature deposited a-SiC using the Hall effect measurements techniques.
- Application of intrinsic a-SiC thin films in contact barrier diodes.
- Calculation of mobility and lifetime of the a-SiC using a simple model of SCLC.

Thin films of a-SiC were prepared *via* the PS-CVD method, at temperatures between 750 °C and 1000 °C. FT-IR spectroscopy was used for providing information on the bonding structure of the synthesized amorphous silicon carbide thin films. Using ERD measurements, it was indicated that the concentration of oxygen in the deposited a-SiC films decreases with increasing temperature, while it is independent of the substrate. The comparison between films deposited at different temperatures indicated a change in the structure and in the composition of the films, especially in terms of hydrogen content. The general narrowing of the IR-absorption bands of the a-SiC films in the 750-1200 cm^{-1} range was indicative of the fact that the structural order in the PS-CVD-deposited a-SiC films augments with increasing temperature of deposition. The conductivity of the films, investigated by CV measurements, also showed an increase with increasing in deposition temperatures. The n-type semiconductor behaviour of the deposited material started at 950 °C, and was clearly dominant in the CV curve obtained at 1000 °C.

Ohmic contacts were obtained on the a-SiC thin films, using a 150 nm-thick Ni film, followed by an annealing step at 800 °C for 2 minutes. Hall measurements were employed for the samples deposited on SiO_2 substrate at 1000 ^{o}C. The average Hall mobility was obtained about μ_H = 34 $cm^2/V.s$. This high value of the mobility was attributed to increased

carbon concentration. The latter affects the conductivity of material by adding more impurity levels in its band gap.

The a-SiC thin films, deposited at 750 °C were considered as an interlayer to modify the barrier height of Ni/p-Si Schottky contact, which resulted lower reverse current and higher breakdown voltage. The optical band gap of a-SiC was determined about 3.6 eV using UV-VIS absorption data. ERD depth profiles were used to estimate the thicknesses of the a-SiC thin films directly under Ni contacts. The current transport via a-SiC were discussed considering IV and CV characteristics. An exponential dependence between the current transport within material with respect to the applied voltage at low voltage bias and space-charge-limited current characteristic at higher voltage bias were found. The actual relationship between current and voltage was found by fitting in high voltage region of IV curves consistent with the theory of SCLC. The ideality factor and barrier height of contact barrier devices were obtained by analysing the IV curves. However, the CV analysis was used to obtain carrier concentration and space-charge width in silicon substrate. Linear dependence of A^2/C^2 to the bias voltage showed that the a-SiC/p-Si is abrupt. The equilibrium carrier density in a-SiC layer were estimated from 2.66×10^{15} cm^{-3} to 5.77×10^{15} cm^{-3} using CV characteristics.

The electric fields in the crystalline substrate and in the amorphous interlayer, and the effective mobility and injected carrier lifetime in the amorphous layer were calculated from IV characteristics, using the SCLC model. The effective hole mobility of a-SiC varied between 10^{-4} and 10^{-7}, effect attributed to the variation in defect-density in different samples. It was mentioned that the switching time of the thin film device is not limited by the low mobility of the a-SiC layer, due to the exponential dependence of V_{sc} on V_a at low forward bias.

The results obtained in this work shows that a-SiC thin film prepared from a polymeric solid source using a fast and low cost method has the potential to be applied in various electronic devices, according to the deposition temperature. The a-SiC thin film deposited at low temperature could be applied as the passivation layer, hydrogen source in solar cells, low

dielectric material in metal/insulator/metal (MIM) and coating material. High temperature deposited thin films could be applied as an n-type semiconductor material in electronic devices such as thin film transistors. As the future works, the following studies are suggested:

- Determination of density of the trap states in a-SiC thin film and at the interface of the a-SiC/c-semiconductors could be the next step in the characterization of this material.
- Experimental determination of a-SiC properties such as electron affinity and impurity level and concentration that are needed for numerical study on a-SiC thin films.
- Numerical simulation of a-SiC behaviour when is applied at different microelectronic devices.

REFERENCES

Adriaenssens, G. J.,and ö. Öktü (1993). "Electronic and Optoelectronic Materials for the 21st Century", *Proceeding of the 7th international school on condensed matter physics*, p. 169-173.

Amato, G. and F. Giorgis (1993). "Accurate reconstruction of the density of states in a-Si:H by constant photocurrent method and photothermal deflection spectroscopy", *Journal of Applied Physics*, vol. 74, p. 3956-3961.

Baylay, P.A., A.K. Browne, J.M. Marshal, R.A.C.M.M. Van Saaij, and A.R. Hepburn (1993). "Study of the temperature and field dependence of electron drift mobility in a-SiC:H using the time-of-flight technique", *Elsevier Science Publishers B.V.*, p. 522-524.

Bolognesi, A., A. Di Carlo, P. Lugli, T. Kampen, D. R. T. Zahn (2003). "Experimental investigation and simulation of hybrid organic/inorganic Schottky diodes", *Journal of Physics: Condensed Matter,* vol. 15, n°. 38, p. S2719-S2728.

Brodsky, M. H. (1985). *Topics in applied physics: amorphous semiconductors*, Springer-Verlag, New York, 347 p.

Buget, U. and G. T. Wright (1967). "Space-charge-limited current in silicon", *Solid-State Electron*, vol. 10, p. 199-207.

Bullot, J., and M. P. Schmit (1987). "Physics of Amorphous Silicon-Carbon Alloys", *Physica Status Solidi* B, vol. 143, p. 345-418.

Chen, Y. A., J. K. Chen, W. C. Tsay, L. H. Laih, J. W. Hong, and C. Y. Cheng (1996). "Double Graded-Gap Hydrogenated Amorphous Silicon Carbide Thin-Film Light-Emitting Diode with Composition-Graded N Layer and Carbon-Increasing P Layer", *Japanese Journal of Applied Physics*, vol. 35, 1018-1021.

Chew, K., Rusli, M. B. Yu, S. F. Yoon, V. Ligatchev, J. Ahn (2001). "Density of gap states in amorphous hydrogenated silicon carbide determined using high-frequency capacitance-voltage measurement technique", *Diamond and Related Materials,* vol. 10, p. 1273-1277.

Cho, N. I., Y. Choi, and S. J. Noh (2006). "Plasma assisted process for deposition of silicon carbide thin films", *Current Applied Physics*, vol. 6, p. 161-165.

Cho, N. I., S. Vlaskina, C. K. Kim (2002). "Electrophysical analysis of SiC films grown onto silicon substrates", *Advances in Technology of Materials and Materials Processing Journal*, vol. 4, p. 96-99.

Cho, S.-M., H. M'Saad, L. Zhang, Z. Li, (2000). "Low dielectric constant material deposited by HDP-CVD for barrier and etch stop application", *Electrochemical Society Proceeding*, p. 48-54.

Cho, H. S., W. S. Hong, N. Palaio, J. Kadyk, K. B. Luk, and V. Perez-Mendez (1996). "Microgap gas chamber studies", *IEEE Transactions on Nuclear Science*, vol. 43, p. 1227-1231.

Choi, W. K. (2001). "Optical, structural, and electrical properties of amorphous silicon carbide films" *Silicon-Based Materials and Devices, Volume 1: Materials and Processing*, Academic Press, p. 1-71.

Choi, W. K., N. B. Chong, L. S. Tan, and L. J. Han (2000). "Effects of RF power and annealing on the electrical and structural properties of sputtered amorphous silicon carbide films", *Material Science Engineering B*, vol. 72, p. 132-134.

Cocorullo, G., G. Della Corte, I. Rendina, A. Rubino, and E. Terzini (1996). "Thermo-optical modulation at λ=1.5 μm in an α-SiC-α-Si-α-SiC planar guided-wave structure", *IEEE Photonics Technology Letters*, vol. 8, n° 7, p. 900-902.

Cros, B., R. Berjoan, C. Monteil, E. Gat, N. Azema, D. Perarnau, and J. Durand (1992). "Limitations on AES quantitative analyses of plasma deposited ceramics", *Journal de Physique III (Paris)*, vol. 2, n° 8, p. 1373-1380.

Deichelis, F., G. Crovini, C. F. Pirri, E. Tresso, R. Galloni, R. Rizzoli, C. Summonte, and P. Rava (1995). "Optimization of relevant deposition parameters for high quality a-SiC:H films", *Solar Energy Materials and Solar Cells,* vol. 37, p. 315-321.

Demichelis, F., C. F. Pirri, E. Tresso, G. Della Mea, V. Rigato, and P. Rava (1991). "Physical properties of undoped and doped hydrogenated amorphous silicon carbide", *Semiconductor Science Technology*, vol. 6, p. 1141-1146.

Deng, J., J. M. Pearce, R. J. Koval, V. Vlahos, R. W. Collins, and C. R. Wronski (2003). "Absence of carrier recombination associated with the defect pool model in intrinsic amorphous silicon layers: Evidence from current-voltage characteristics on p-i-n and n-i-p solar cells", *Applied Physics Letters*, vol. 82, n°. 18, p. 3023-3026.

Dismukes, J. P., J. W. Johnson, J. S. Bredly, J. M. Miller (1997). "Chemical Synthesis of Microporous Nonoxide Ceramics from Polysilazanes", *Chemistry of Materials*, vol. 9, p. 699-706.

Dutta, P. S., A. K. Sreedhar, and H. L. Bhat (1995). "Current transport properties of metal/hydrogenated amorphous silicon/CaSb structures", *Applied Physics Letters*, vol. 67, n°. 7, p. 1001-1003.

Eickhoff, M., H. Möller, J. Stoemenos, S. Zappe, G. Kroetz, and M. Stutzmann (2004). "Influence of crystal quality on the electronic properties of n-type 3C-SiC grown by low temperature low pressure chemical vapour deposition", *Journal of Applied Physics*, vol. 95, p. 7908-7917.

El Khakani, M. A., and M. Chaker (1993). "Physical properties of the x-ray membrane materials", *Journal of Vacuum Science and Technology B*, vol. 11, p. 2930-2937.

Endo, K., T. Tatsumi (1996). "Fluorinated amorphous carbon thin films grown by helicon plasma enhanced chemical vapor deposition for low dielectric constant interlayer dielectrics", *Applied Physics Letters*, vol. 68, n°. 20, p. 2864-2866.

Folsch, J., H. Rubel and H. Schade (1992). "Change in bonding properties of amorphous hydrogenated silicon-carbide layers prepared with different gases as carbon sources", *Applied Physics Letters*, vol. 61, p. 3029-3031.

Forrest, S. R., M. L. Kaplan, and P. H. Schmidt (1984). "Organic-on-inorganic semiconductor contact barrier diodes, I. Theory with applicatios to organic thin films and prototype devices, *Journal of Applied Physics*, vol. 55, n°. 6, p. 1492-1507.

Fu, Z., J. Ning, B. Yang, W. Wu, H. Pan and P. Xu (2003). "Stable ultraviolet photoluminescence from sol-gel silica containing nano-sized SiC/C powder" *Material Letters*, vol. 57, n° 13-14 p. 1910-1914.

Gerault, J. P., P. Morancho, and G. Constant (1984). "Photoluminescence et propriétés optiques d'alliages SixC1-x amorphes préparés par depôt chimique en phase vapeur", *Philosophical Magazine B*, vol. 49, p. 11-26.

Gerault, J. P., P. Morancho, G. Constant, P. Mazerolls, J. J. Ehrhardt, and M. Alnot (1983). "X-ray photoelectron spectroscopy and Raman spectroscopy investigations of amorphous $Si_xC1_x(H)$ coatings obtained by chemical vapour deposition from thermally labile organosilicon compounds", *Thin Solid Films,* vol. 101, p. 83-96.

Gerault, P., P. Morancho, G. Constant, P. Mazerolls, and G. Manuel (1982). "Mass spectrometric investigation of the thermal decomposition of various organosilicon compounds in $Si_xC_{1-x}(H)$ chemical vapour deposition", *Journal of Analytical and Applied Pyrolysis*. Vol. 4, p. 59-72.

Gu, Q., Q. Wang, and E. A. Schiff (1994). "Hole drift mobility measurements in amorphous silicon-carbon alloys", *Journal of Applied Physics,* vol. 76, n°. 4, p. 2310-2316.

Han, S. Y., J.-Y. Shin, B.-T. Lee, and J.-L. Lee (2002). "Microstructural interpretation of Ni ohmic contact on n-type 4H–SiC", *Journal of Vacuum Science Technology B*, vol. 20, p. 1496-1500.

Han, M., Y. Matsomoto, G. Hirata, H. Okamoto, and Y. Hamakawa (1989). "Characterization of boron doped μc-SiC/c-Si heterojunction solar cells", *Journal of Non-Crystalline Solids,* vol. 115, p. 195-197.

Herman, T. E., J. C. Blair, and C. A. Mead (1968). "Electrical conduction through thin amorphous SiC films", Thin Solid Films, vol. 2, p. 79-93.

Hiramoto, M., T. Miyao, and M. Yokoyama (1990). "Up-conversion of red light to green by a new type of light transducer using organic electroluminescent diode combined with photoresponsive amorphous silicon carbide", *Applied Physics Letters*, vol. 58, p. 1148-1150.

Hong, W. S., H. S. Cho, S. Biagi, F. Retiere, J. Kadyk, V. Perez-Mendez, N. Palaio, and J. Vujic (1998). "Gas avalanche pixel detectors with amorphous silicon carbide (a-Si:C:H) overcoating", *IEEE Transactions on Nuclear Science,* vol. 45, p. 252-257.

Jang, J. H., and K. S. Lim (1997). "Etching and passivation effects on boron-doped amorphous silicon carbide p layer of amorphous silicon solar cell by hydrogen treatment using a mercury-sensitized photochemical vapour deposition method", *Applied Physics Letters*, vol. 71, n°. 13, p. 1846-1849.

Janz, S., S. Reber, S. W. Glunz (2006). Amorphous SiC: Applications for silicon solar cells", *European Photovoltaic Solar Energy Conference and Exhibition (Dresden)*, p. 4-8.

Jung, C.-K., D.-C. Lim, H.-G. Jee, M.-G. Park, S.-J. Ku, K.-S. Yu, B. Hong, S.-B. Lee, and J.-S. Boo (2002). "Hydrogenated amorphous and crystalline SiC thin films grown by RF-PECVD and thermal MOCVD; comparative study of structural and optical properties", *Surface and Coating Technology*, vol. 171, n°. 1-3, p. 46-50.

Jwo, S. C., M. T. Wu, Y. K. Fang, and C. Y. Chag (1988). "Amorphous silicon/silicon carbide superlattice avalanche photodiodes", *IEEE Transactions Electron Devices*, vol. 35, p. 1279-1283.

Jwo, S. C., and C. Y. Chang (1986). "Amorphous silicon/silicon carbide heterojunction bulk unipolar diodes (HEBUD)", *IEEE Electron Device Letters*, vol. 7, p. 689-691.

Kaneko, T., D. Nemoto, A. Horiguchi and N. Miyakawa (2005). "FTIR analysis of a-SiC:H films grown by plasma enhanced CVD" *J. Cryst. Growth*, vol. 275, p.1097-1101.

Kanicki, J. (1991). *Amorphous and Microsrystalline Semiconductor Devices*, Artech House, 784 p.

Kho, J., K. Moon, G. Nouet, Ruterana, K. Kim (2001). "Boron-rich boron nitride (BN) films prepared by a single spin-coating process of a polymeric precursor", *Thin Solid Films*, vol. 389, p. 78-83.

Klazes, R. H., M. H. L. M. Van den Broek, J. Bezemer, and S. Radelaar (1982). "Determination of the optical bandgap of amorphous silicon", *Philosophie Magazine*, vol. 45, p. 377-383.

Kortright, J. B. and D. L. Windt, (1988) "Amorphous silicon carbide coatings for EUV optics", *Appl. Opt.* Vol. 27, p. 2841-2846.

Kortright, J. B., P. Plag, R. C. C. Pereta, P. L. Cowan, D. W. Lindle, and B. Karlin (1988). "Multilayer-coated mirrors as power filters in synchrotron radiation beam lines", *Nuclear Instruments and Methods*, vol. 266, p. 452-456.

Krotz, G., G. Muller, G. Derst, Ch. Wilbertz, and S. Kalbitzer (1994). "Thin-film SiC as an optical and optoelectronic material", *Diamond and Related Materials*, vol. 3, p. 917-921.

Kruangam, D., D. Deguchi, T. Toyama, H. Okamoto, and Y. Hamakawa (1988). "Carrier injection mechanism in an a-SiC p-i-n junction thin-film", IEEE Trans. Electron Dev., vol. 35, p. 957-965.

Kruangam, D., T. Endo, G. P. Wei, S. Nomomura, H. Okamoto, and Y. Hamakawa (1985). "A study of visible-light injection-electroluminescence in a-SiC/p-i-n diode", *Journal of Non-Crystalline Solids*, vol. 77-78, p. 1429-1432.

Kuwano, Y., M. Ohnishi, S. Tsua, Y. Hamkawa (1989). "Properties and structure of a-SiC:H for high-efficiency a-Si solar cell", *Journal of Applied Physics*, vol. 53, p. 5273-5282.

Lang, W., P. Steiner, U. Schaber, and A. Richter (1993). "A thin film bolometer using porous silicon technology", *Proceedings of the 7th International Conference on Solid-State Sensors and Actuators A*, vol. 43, p. 185-187.

Lang, D. V., J. D. Cohen, and J. P. Harbison (1982). "Measurement of the density of gap states in hydrogenated amorphous silicon by space charge spectroscopy", *Physical Review B*, vol. 25, n°. 8, p. 5285-5320.

Lau, S. P., J. M. Marshal, T. E. Dyer, A. R. Hepburn, and J. F. Davis (1993). "a-SiC:H thin film visible light-emitting diodes with highly conductive wide band gap a-SiC:H as the carrier injection layers", *Journal of Non-Crystalline Solids*, vol. 164-166, p. 813-816.

Li, X., T.K.S. Wong, Rusli, D. Yang (2003). "Structural and electronic properties of low dielectric constant carbon rich amorphous silicon carbide", *Diamond and related materials*, vol. 12, p. 963-967.

Li, Y. M., I. An, M. Gunes, M. Wakaqi, C. R. Wronski, R. M. Dawson, and R. W. Collins (1993). "Effects of Gas Phase Hydrogen Dilution on the Nucleation, Growth and Interfaces of a-$Si_{1-x}C_x$:H Alloys", *Material Research Society Symposium Proceeding*, vol. 297, p. 31-36.

Li, Y. M., A. Catalano, and B. F. Fieselmann (1992). "Film and solar cell properties of a-SiC:H alloys", *Material Research Society Symposia Proceeding - Amorphous Silicon Technology*, p. 923-928.

Lin, W. L., H. K. Tsai, S. C. Lee, W. J. Sah and W. J. Tzeng (1987). "Identification of infrared absorption peaks of amorphous silicon-carbon alloy by thermal annealing", *Applied Physics Letters*, vol. 51, p. 2112-2114.

Lu, Y., I. An, M. Gunes, M. Wakagi, C. R. Wronski, and R. W. Collin (1993). "Effect of gas phase hydrogen-dilution on the nucleation, growth, and interfaces of a-Si1-xCx:H" *Material Research Society Symposia Proceeding - Amorphous Silicon Technology,* p. 31-36.

Magob, C. J. and W. E. Kingery (1968). "Preparation and Properties of Noncrystalline Silicon Carbide Films", *Journal of Applied Physics*, vol. 39, p. 3640-3645.

Mahajan, A. M., L. S. Patil, J. P. Bange and D. K. Gautam (2004). "Growth of SiO2 films by TEOS-PECVD system for microelectronics applications", *Surf. Coat. Technol.*, vol. 183, p. 295-300

Mahan, A. H., B. Von Roedern, D. J. Williamson and A. Madan (1985). "Evidence for graphitic-type bonding in glow discharge hydrogenated amorphous silicon carbon alloys", *Journal of Applied Physics*, vol. 57, p. 2717-2720.

Mandel, T., M. Frischholz, R. Helbig (1994). "Gap-state measurements on diamond-like carbon films", *Applied Physics Letters*, vol. 64, p. 3637-3643.

Marsal, L. F., J. Pallares, X. Correig, A. Orpella, D. Bardes, and R. Alcubilla (1999). "Analysis of conduction mechanisms in annealed n-Si1 – xCx:H/p-crystalline Si heterojunction diodes for different doping concentrations", *Journal of Applied Physics*, vol. 85, p. 1216-1221.

Marsal, L. F., J. Pallarès, X. Correig, M. Dominguez, D. Bardès, J. Calderer, and R. Alcubilla (1997). "Electrical properties of PECVD amorphous silicon –carbon alloys from amorphous-crystalline heterojunctions", *Diamond an Related Materials*, vol. 6, p. 1555-1558.

Martin, I., M. Vetter, A. Orpella, J. Puigdollers, and A. Cuevas (2001). "Surface passivation of p-type crystalline Si by plasma enhanced chemical vapor deposited amorphous SiC_x:H films", *Applied physics letters*, vol. 79, p. 2199-2201.

Mastelaro, V., A. M. Flank, M. C. A. Fantini, D. R. S. Bittencourt, M. N. P. Carreno, and I. Pereyra (1997). "On the structural properties of a-$Si_{1-x}C_x$:H thin films", *Journal of Applied Physics*, vol. 79, p. 1324-1329.

Matsuda, A., T. Yamaoka, S. Wolff, M. Koyama, Y. Imanishi, H. Ktaoka and H. Matsuura (1986). "Preparation of highly photosensitive hydrogenated amorphous Si-C alloys from a glow-discharge plasma", *Journal of Applied Physics,* vol. 60, p. 4025-4027.

Matsuura, H., Z. E. Smith, A. Matsuda (1989). "Midgap-state profiles in undoped amorphous-silicon-based alloys", *Philosophical Magazine Letters*, vol. 59 (2), p. 109-114.

Matsuura, H. (1989). "Hydrogenated amorphous silicon/crystalline silicon heterojunctions: properties and applications", *IEEE Transaction Electron Devices*, vol. 30, n°. 12, p. 2908.

Matsuura, H. (1988). "Density-of-state distribution for undoped a-Si:H and a-$Si_{1-x}Ge_x$:H determined by transient heterojunction-monitored capacitance method", *Japanese Journal of Applied Physics*, vol. 27, n°. 4, p. 516-518.

Matsuura, H. (1988). "Density of mid-gap states for undoped a-$Si_{1-x}Ge_x$:H and a-Si:H determined by steady-state heterojunction-monitored capacitance method", *Japanese Journal of Applied Physics*, vol. 27, n°. 4, p. 513-515.

Megafas, L., N. Georgoulas, and A. Thanallakis (1992). "Electrical properties of a-SiC/c-Si(p) heterojunctions", *Semiconductor Science Technology,* vol. 7, p.1363-1368.

Miller, L. S. and J. B. Mullin (1991). *Electronic Materials from Silicon to Organics*, Springer, New York, 542 p..

Mott, N. F. and E. A. Davis (1979). *Electronic processes in Non-Crystalline Materials*, Oxford, Univ. Press, London.

Muller, G., G. Krotz, and E. Niemann (1995). "SiC for sensors and high-temperature electronics", *Sensors Actuators*, vol. 43, p. 259-268.

Muller, G. (1997). "Colour sensing applications of hydrogenated amorphous silicon carbide", *Diamond and Related Materials*, vol. 6, p. 1542-1546.

Munekata, H., S. Murasato, and H. Kukimoto (1980). "White photoluminescence of amorphous silicon-carbon alloy prepared by glow-discharge decomposition of tetramethylsilane", *Applied Physics Letters*, vol. 37, p. 536-538.

Nebel, C. E. and R. A. Street (1993). "Hall experiments and interpretation in a-Si:H and a-SiC:H", *Elsevier Science Publishers B. V.*, p. 449-452.

Nelson, W. E., F. A. Halden, and A. Rosengreen (1966). "Growth and Properties of β-SiC Single Crystals", *Journal of Applied Physics*, vol. 37, p. 333-338.

Nishikawa, S., H. Hashimoto, M. Shikamoto, K. Horikoshi, M. Aoki, K. Arima, J. Ychikosi, M. Morita (2006). "Photo current through SnO_2/SiC/p-Si(100) structures", *Thin Solid Films*, vol. 508, p. 385-388.

O'Connor, J. R., and J. Smiltens eds. (1960), *Silicon Carbide: A High Temperature Semiconductor*, Pergamon Press, Oxford, 496 p.

Paul, B. C., M. Satyam, and A. Selvarajan (1999). "A novel method of optical detection using a capacitive device", *IEEE Transactions on Electron Devices*, vol. 46, p. 324-328.

Ramakrishnan, P. A., Y. T. Wang, D. Balzar, L. An, C. Haluschka, R. Reidel, A. M. Hermann (2001). "Silicoboron–carbonitride ceramics: A class of high-temperature, dopable electronic materials", *Applied Physics Letters*, vol. 78, p. 3076-3078.

Rhoderick, E. H. and R. H. Williams (1988). *Metal-Semiconductor Contacts*, Clarendon, Oxford, England, 252 p.

Rizk R. B., Kaloyeros A. E., Williams W. S., Finnegan N., and C. Kozolowsky, (1987), "Sputtered films of amorphous hydrogenated silicon carbide" *Novel Refractory Semiconductors Symposium. Proc.* , p. 295-300.

Rose, A. (1963). *Concepts in photoconductivity and Allied Problems*, Interscience Publishers, New York, 168 p.

Sasaki, G., S. Fujita, and A. Sasaki (1982). "Gap-States measurement of chemically vapor-deposited amorphous silicon: High-frequency capacitance-voltage method", *Journal of Applied Physics*, vol. 53, n°. 2, p. 1013-1017.

Sasaki, T., G. Sasaki, and A. Sasaki (1982). "Some problem in determination of gap-state density in amorphous silicon", *Solar Energy Materials*, vol. 8, p. 293-302.

Scarlete, M., and C. Aktik, International Patent No. WO 03/100123 A1, 4 Dec. 2003.

Scarlete, M., I. S. Butler, and J. F. Harrod (1995). "Nitrogenation of Silicon Carbide Layers Deposited on Silicon Single-Crystal Wafers via Pyrolysis of Poly(methylsilane)", *Chemistry of Materials*, vol. 7, p. 1214-1220.

Scarlete, M., S. Brienne, I. S. Butler, and J. F. Harrod (1994). "Infrared spectroscopic study of thin films of poly(methylsilane), its oxidation, and its transformation into poly(carbosilane) on the surfaces of silicon single-crystal wafers", *Chemistry of Materials,* vol. 6, p. 977-982.

Schiff, E. A., A. Madan, M. J. Thompson and K. Tanaka (1993). "Amorphous silicon technology", *Material Research Science Symposium Proceeding*, vol. 297 p. 1066.

Schlichting, J. (1980). "Chemical Vapor Deposition of Silicon Carbide", *Powder Metallurgy International,* vol. 12, p. 141-147.

Schroder, D. K. (1990). *Semiconductor material and device characterization*, John Wiley & Sons, Inc., 624 p.

Shen, D. S., S. T. Kowei, and C. A. Eldering (1995). "Amorphous silicon thin-film photodetectors for optical interconnection", *Optical Engineering*, vol. 34, p. 881-886.

Shin, N. F., T. Y. Chen, T. S. Jen, J. W. Hing, and C. Y. Chang (1993). "Hydrogenated amorphous silicon carbide double graded-gap p-i-n thin-film light-emitting diodes", *IEEE Electron Device Letters*, vol. 14, p. 453-455.

Shiozawa, J., Y. Kasai, Y. Mikata, K. Yamabe (1995). "The Formation of Boron-Doped Polycrystalline Si with Extremely Low Resistivities at Low Temperatures", *Journal of Electrochemical Society*, vol. 141, p. 1334-1338.

Sichanugrist, P., M. Konagai, and K. Takahashi (1984). "Theoretical analysis of amorphous silicon solar cells: effects of interface recombination", *Jounal of Applied Physics*, vol. 55, n°. 4, p. 1155-1162.

Sze, S. M. (1981). *Physics of semiconductor Devices*, 2nd edition, Wiley-Interscience, New York, 880 p.

Sze, S. M. and H. K. Gummel (1966). "Appraisal of semiconductor-metal-semiconductor transistor", *Solid-State Electronics*, vol. 9, p. 751-769.

Tabata, A., T. Nakajima, T. Mizutani and Y. Suzuoki (2003). "Preparation of wide-gap hydrogenated amorphous silicon carbide thin films by hot-wire chemical vapor deposition at a low tungsten temperature", *Japanese Journal of Applied Physics*, vol. 42, p. L10-L12.

Takahashi, J., N. Ohtani, M. Katsumo, and S. Shinoyama (1997). "Sublimation growth of 6H- and 4H-SiC single crystals in the $[1\bar{1}00]$ and $[11\bar{2}0]$ directions", *Journal of Crystal Growth,* vol. 181, p. 229-240.

Tang, Y. and R. Braunstein (1995). "Effects of deposition conditions on transport properties of intrinsic hydrogenated amorphous silicon and hydrogenated amorphous silicon carbide films investigated by the photomixing technique", *Applied Physics Letters*, vol. 66, n° 6, p. 721-723.

Uokomichi, H., T. Tatsumi, A. Masuda (1998). "Changes in structure and nature of defects by annealing of fluorinated amorphous carbon thin films with low dielectric constant", *Applied Physics Letters,* vol. 72, n°. 21, p. 2704-2706.

Van der Pauw, L. J. (1958). "A method of measuring specific resistivity and Hall Effect of discs of arbitrary shapes", *Philips Res. Repts,* vol. 13, p. 1-9.

Van der Pauw, L. J. (1958). "A method of measuring the resistivity and Hall coefficient on lamellae of arbitrary shape", *Philips Tech. Rev.*, vol. 20, p. 220-224.

Vilan, A., A. Shanzer, and D. Cahen (2000). "Molecular control over Au/GaAs diodes", *Nature*, vol. 404, p. 166-168.

Von Der Linden, M. B., R. E. I. Schropp, R. Balkema, R. A. C. M. M. Van Swaaij, J. Daey Ouwens, W. G. J. H. M. Van Sark, J. Bezemer and W. F. Van Der Weg (1992). "Thickness related effects in p-type amorphous silicon thin films", *Proceedings of the 11th European Photovoltaic Solar Energy Conference*, Harwood Academic Publishers, Chur, Switzerland, p. 684-687.

Wang, Q., E. A. Schiff, and Y. Li (1993). "Electron time-of-flight measurements in a-$Si_{1-x}C_x$:H", Materials Research Society Symposium Proceedings, vol. 297, p. 419-424.

Weider, H., M. Cardona, and R. Guarnieri (1987). "Physics of Amorphous Silicon-Carbon Alloys", *Physica Status Solidi B*, vol. 143, 345-418.

Weinreich, O. A. and A. Ribner (1968). "Optical and Electrical Properties of SiC Films Prepared in a Microwave Discharge", *Journal of Electrochemical Society*, vol. 115, p. 1090-1092.

Wieder, H., M. Cardona, and R. Guarnieri (1979). "Vibrational spectrum of hydrogenated amorphous Si-C films", *Physica Status Solidi B*, vol. 92, p. 99-112.

Wind, J., G. Krotz, R. Schmiedgen, W. Legner, I. Binder, Y. Hechtenberg, and G. Muller (1993). "Colour detection using amorphous semiconductor thin-film alloys", *Sensors Actuators A*, vol. 36, p. 187-192.

Yabe, M., N. Sato, and Y. Seki (1984). "A new silicon nuclear radiation detector using a-Si:H/c-Si heterojunction", *Proceeding of the 4th Sensor Symposium*, Tsukuba, p. 105-107.

Zhuge, L. J., X. M. Wu, Q. Li, W. B. Wang and S. L. Xiang (2004). "Origin of violet photoluminescence in SiO2 films co-doped with silicon and carbon", *Physica E*, vol. 23, p. 86-91.

Zhang, S., L. Raniero, E. Fortunato, L. Pereira, N. Martins, P. Canhola, I. Ferreira, N. Nedev, H. Aguas, R. Martins (2004). "Characterization of silicon carbide thin films prepared by VHF-PECVD technology", *J. Non-Cryst. Solids,* vol. 338-340, p. 530-533.